

ISAPP 2014: Multi-wavelength and multi-messenger
investigation of the visible and dark Universe

High-Energy processes in astronomical sources

Andrii Neronov

University of Geneva

Outline of the three lectures

Lecture 1:

Overview of high-energy sky

Thermal and non-thermal sources

Galactic and extragalactic sources

Particle acceleration / interaction / radiation mechanisms

Shock acceleration and acceleration by large scale electric fields

Synchrotron, inverse Compton, Bremsstrahlung emission by electrons / positrons

Pion production / decay emission from high-energy protons

Lecture 2:

Physics of high-energy sources (selected examples)

Pulsars / pulsar wind nebulae

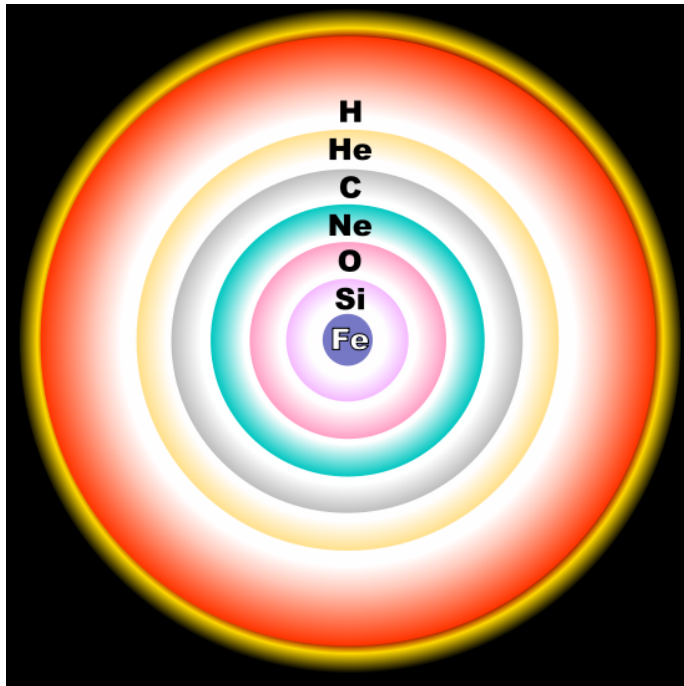
Active galactic nuclei and blazars

The Galactic Center

Lecture 3:

Pulsars and pulsar wind nebulae

Origin of neutron stars



Massive stars end their life with formation of iron core where no nucleosynthesis reaction take place. The dense core is supported against gravity by the pressure of degenerate electron gas

$$\Delta p_e \Delta x \sim 1, \quad m_e (\Delta v_e) \cdot \frac{1}{n_e^{1/3}} \sim 1$$

$$P = n_e p_e v_e \sim n_e^{5/3}$$

Mass-radius relation of the iron core follows from hydrostatic equilibrium condition

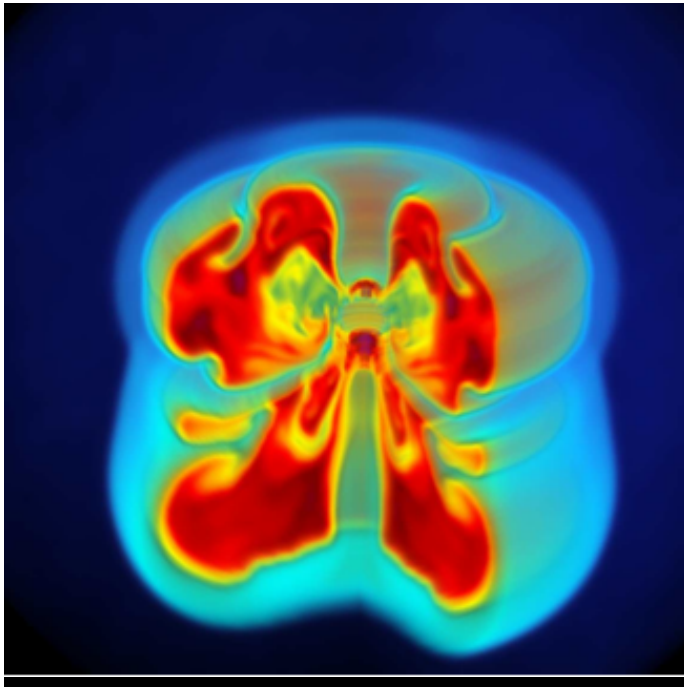
$$\frac{dP}{dr} \sim \frac{P}{R} \sim \frac{n_e^{5/3}}{R} \sim \frac{Y_e^{5/3} M^{5/3}}{m_p^{5/3} R^{8/3}} \sim \frac{G_N M \rho}{R^2}$$

$$R \sim \frac{Y_e^{5/3}}{m_p^{5/3} m_e G_N M^{1/3}}$$

Accumulation of iron in the core leads to contraction of the core and increase of the Fermi velocity up to the speed of light, at the moment when the core mass reaches the “Chandrasekhar mass”

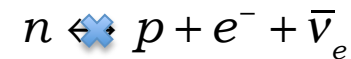
$$M_{Ch} \approx \frac{1}{m_p^2 G_N^{3/2}} \approx 1.4 M_\odot$$

Origin of neutron stars



As soon as the core reaches the Chandrasekhar mass, degenerate electron gas in the core becomes relativistic and its equation of state changes: $P = n_e p_e c \sim n_e^{4/3}$

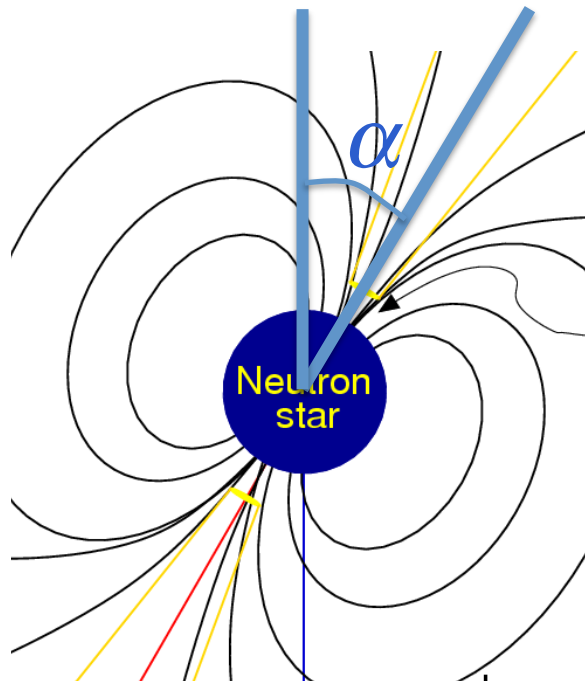
The hydrostatic equilibrium condition has no solution for $M > M_{Ch}$. The core experiences gravitational collapse. The collapse is accompanied by the process of “neutronization”:



The new configuration is supported by the pressure of degenerate neutron gas and is called “**neutron star**”.

Neutron star mass is $M \sim M_{Ch}$. Its size is $R \sim (m_p^{8/3} G_N M^{1/3})^{-1} \sim (m_p^2 G_N^{1/2})^{-1} \approx 10^6 \text{ cm}$. Its density is $\rho \approx M / R^3 \approx 10^{15} \text{ g/cm}^3$. Its rotation period could be estimated from the conservation of angular momentum $R^2 / P = \text{const}$, which gives $P_{NS} = (R / R_*)^2 P_* \sim 1 \text{ ms}$. Its magnetic field could be estimated from the conservation of magnetic flux $BR^2 = \text{const}$. This gives $B_{NS} = (R / R_*)^{-2} B_* \sim 10^{12} \text{ G}$.

Pulsars



A compact star with parameters

$$M \sim M_{Ch}$$

$$R \sim (m_p^{8/3} G_N M^{1/3})^{-1} \sim (m_p^2 G_N^{1/2})^{-1} \approx 10^6 \text{ cm}$$

$$P = (R / R_*)^2 P_* \sim 1 \text{ ms}$$

stores the rotation energy

$$E_{rot} = \frac{I\Omega^2}{2} \approx \frac{4\pi^2 MR^2}{5P^2} \sim 10^{52} \left[\frac{P}{1 \text{ ms}} \right]^{-2} \text{ erg}$$

A rotating magnetic dipole loses energy via dipole radiation, with the energy loss rate

$$-\dot{E}_B = \frac{2}{3} \ddot{u}^2 = \frac{B^2 R^6 \sin^2 \alpha}{6P^4}$$

Dissipation of rotation energy should gradually slow down the rotation of the neutron star

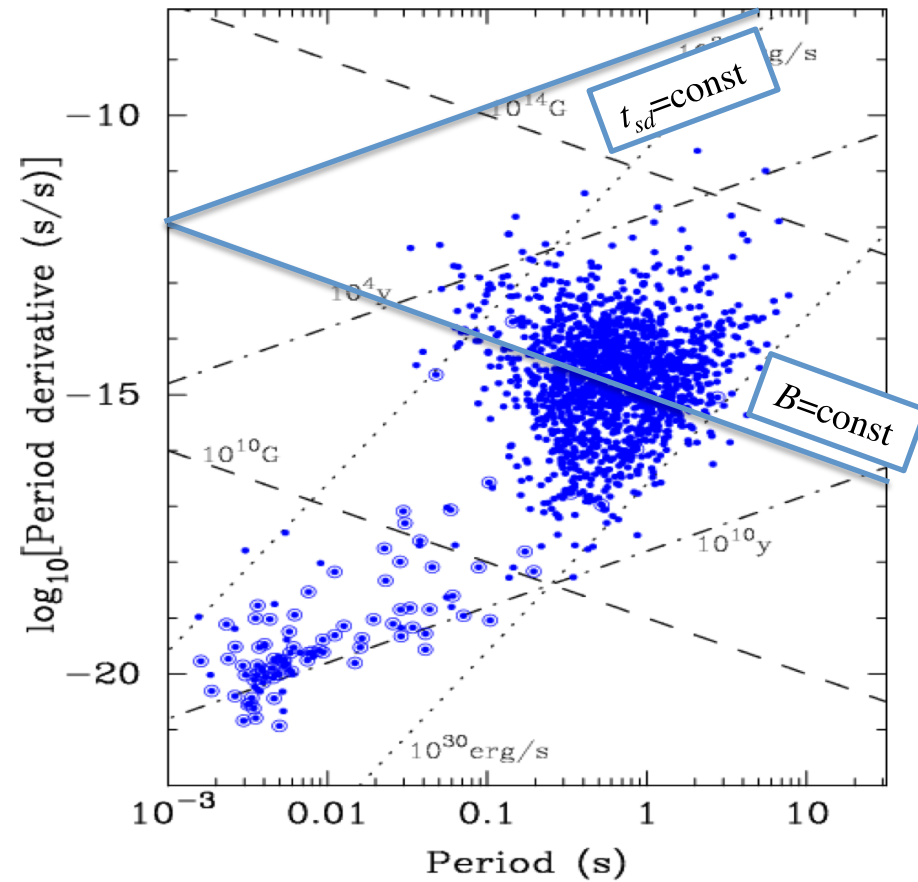
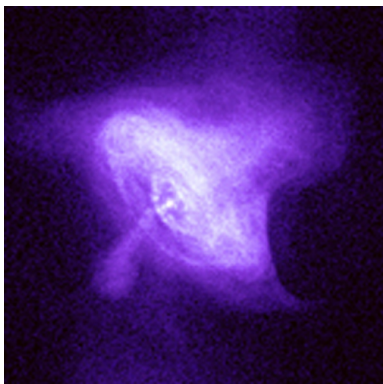
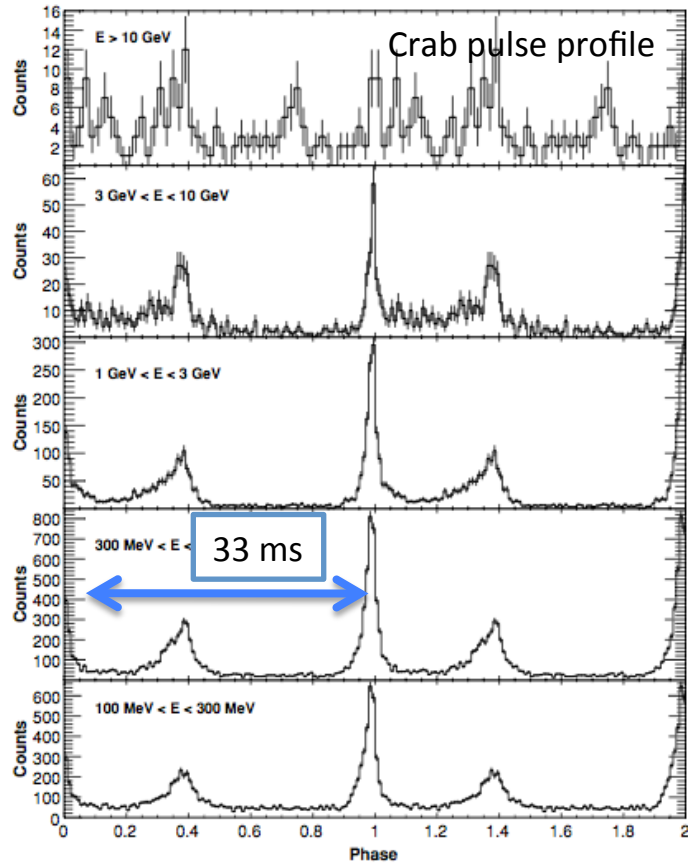
$$-\dot{E}_B = \frac{8\pi^4 B^2 R^6 \sin^2 \alpha}{3P^4} \sim \frac{8\pi^2 MR^2 \dot{P}}{5P^3} = -\dot{E}_{rot}$$

$$\dot{P} \approx \frac{10\pi^2 B^2 R^4}{3MP} \approx 10^{-12} \left[\frac{B}{10^{12} \text{ G}} \right]^2 \left[\frac{P}{1 \text{ ms}} \right]^{-1}$$

Neutron star should slow down its rotation on the time scale

$$t_{sd} = \frac{P}{\dot{P}} \approx 10^{1.5} \left[\frac{B}{10^{12} \text{ G}} \right]^{-2} \left[\frac{P}{1 \text{ ms}} \right]^2 \text{ yr}$$

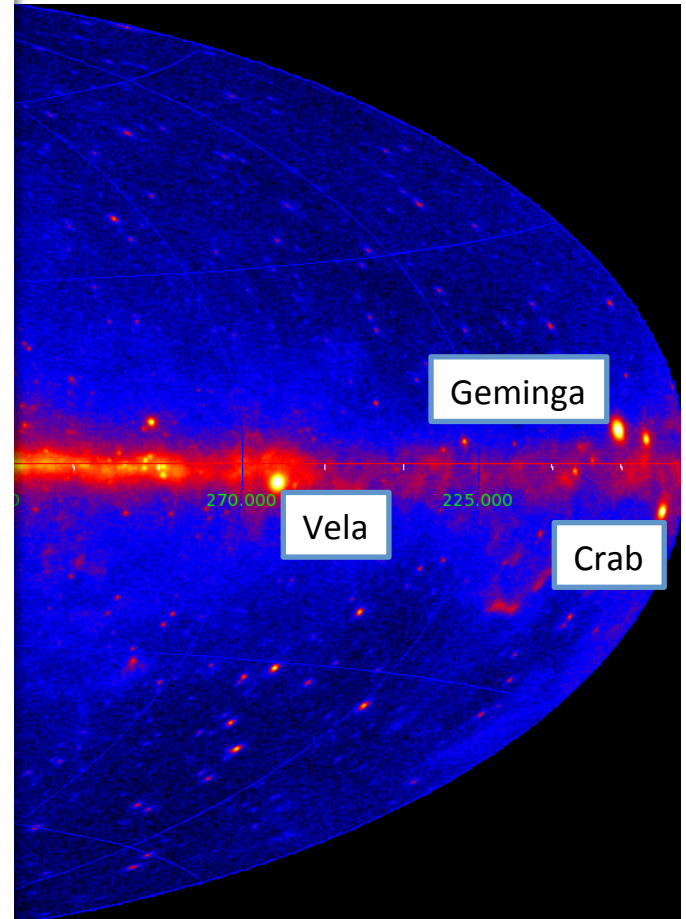
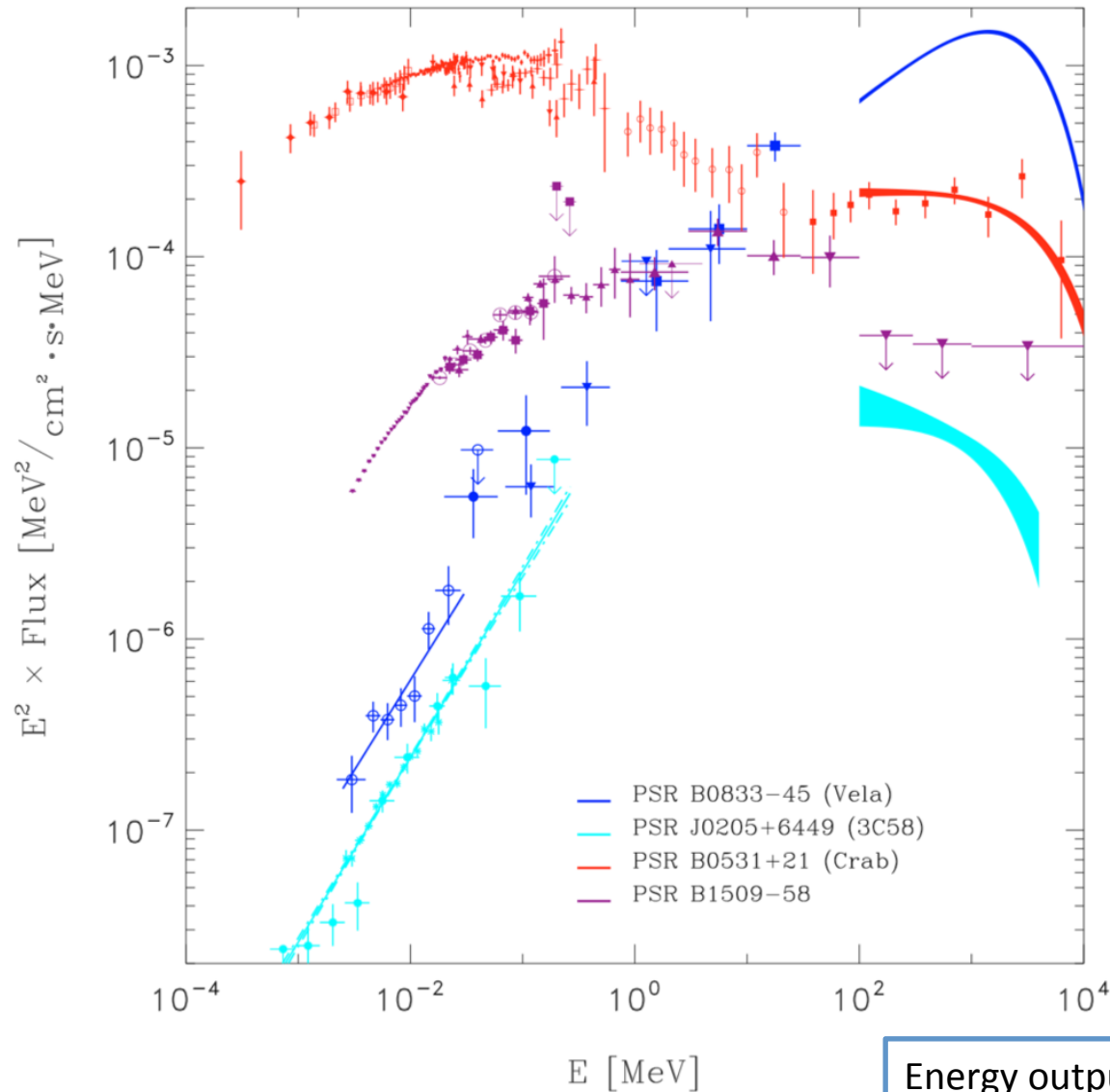
Pulsars



For a neutron star spinning down due to magnetic dipole radiation

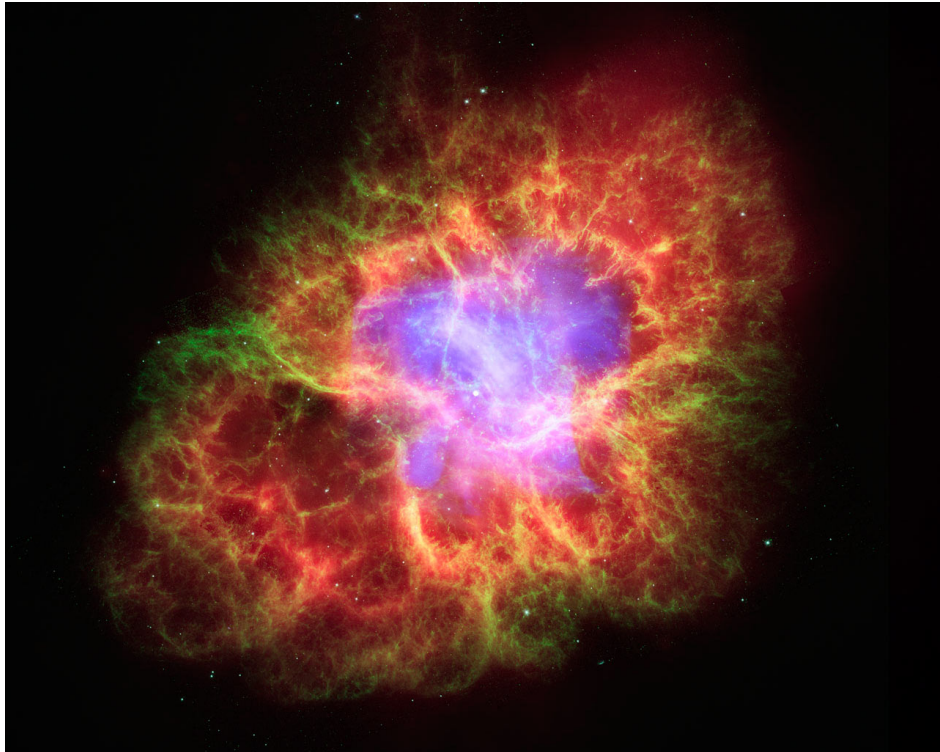
$$\dot{P} \approx \frac{P}{t_{sd}} = \frac{P}{\dot{P}} \approx 10^{-12} \left[\frac{B}{10^{12} \text{ G}} \right]^2 \left[\frac{P}{1 \text{ ms}} \right]^{-1}$$

Pulsars



Energy output of pulsed emission from pulsars is dominated by gamma-ray band

Crab pulsar



Crab pulsar is a powerful source some **2 kpc** away at the place of a supernova explosion recorded by Chinese astronomers in some **10^3 yr** ago.

Its parameters are

$$P \approx 33 \text{ ms} \quad \dot{P} \approx 4 \times 10^{-13} \text{ s/s}$$

The spin-down age is

$$t_{sd} = P / \dot{P} \approx 10^3 \text{ yr}$$

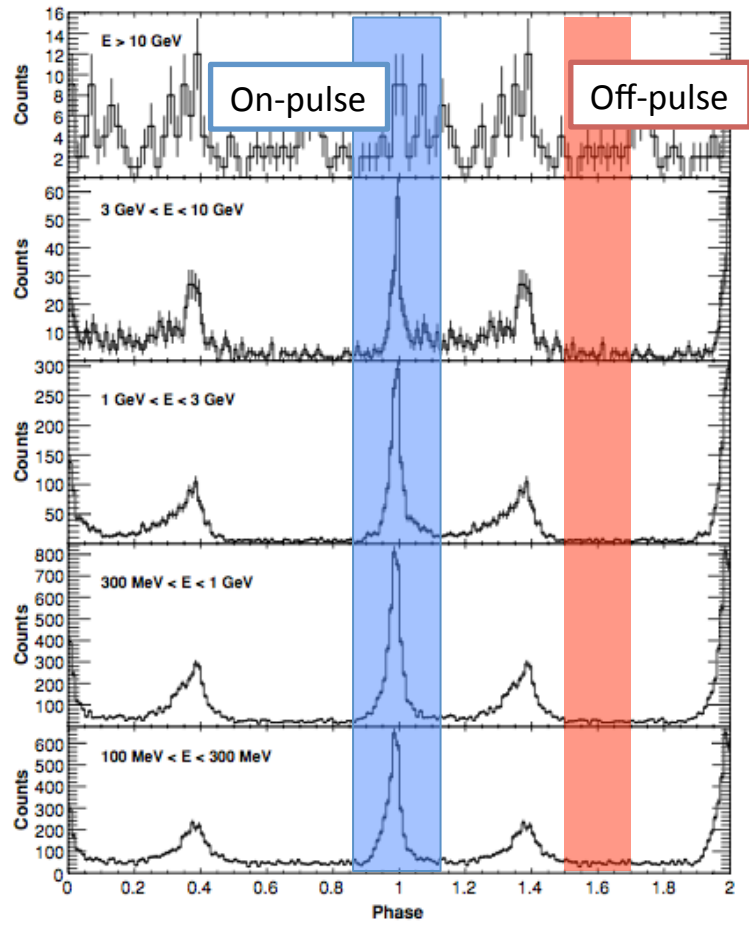
It is the youngest observed pulsar in the Milky Way galaxy.

The spin-down power is

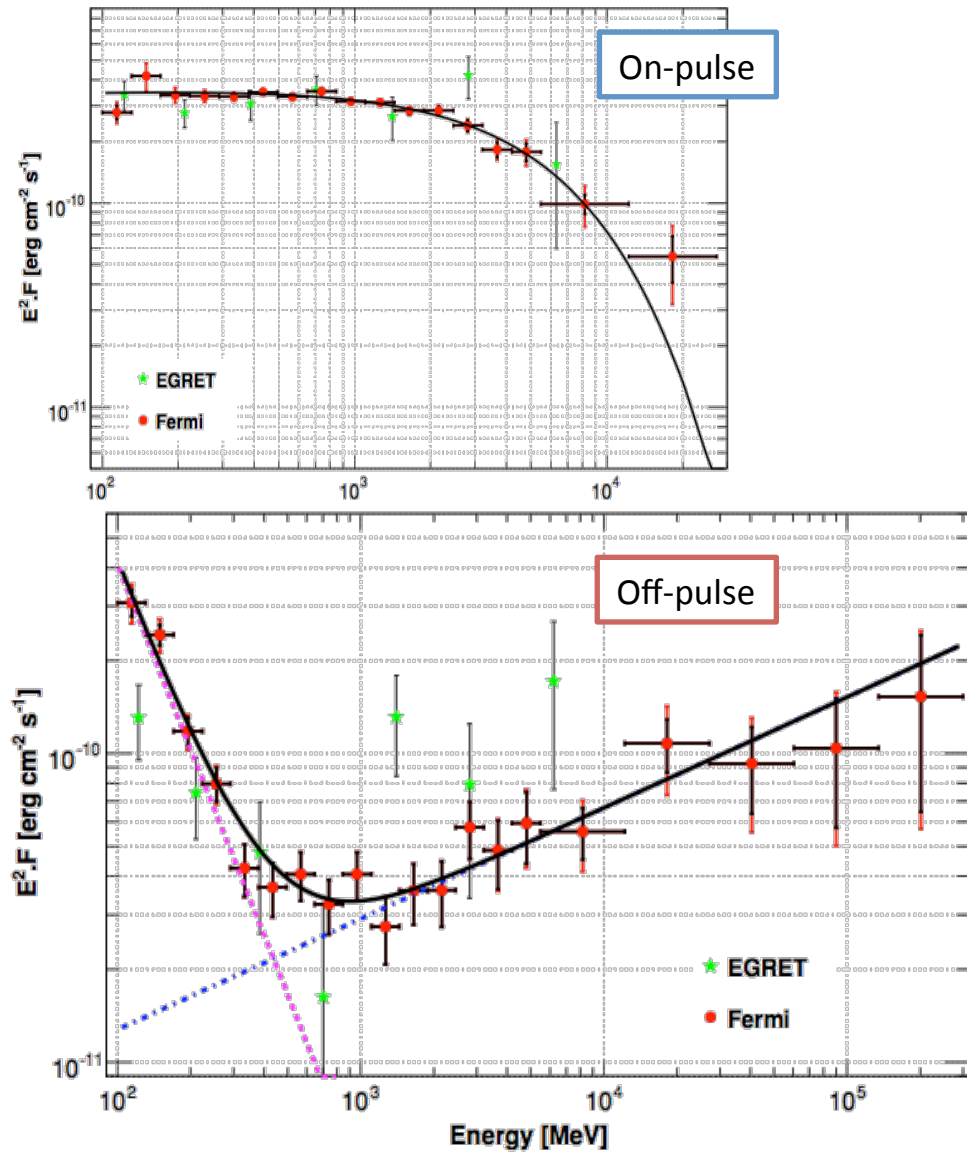
$$\dot{E}_{sd} = \frac{8\pi^2 MR^2 \dot{P}}{5P^3} \approx 10^{38} \text{ erg/s}$$

Only a small fraction of this power is converted into the pulsed emission power. Most of the power is released in a larger scale nebula.

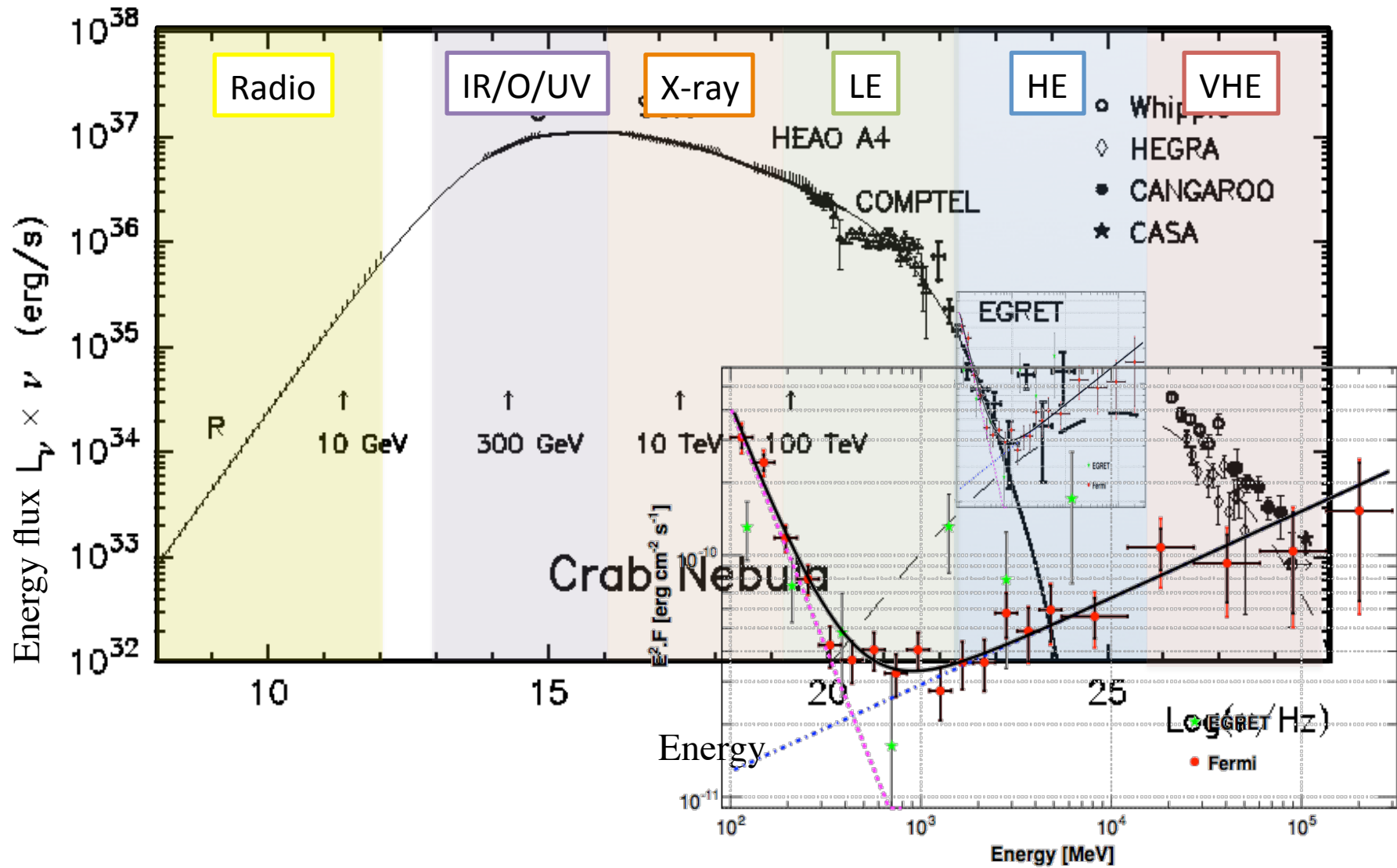
Crab pulsar



Gamma-ray spectrum strongly changes between on- and off-pulse.



Crab Nebula



Pulsars as particle accelerators

Lorentz force leads to charge redistribution at the surface of the neutron star.

Charge redistribution creates an electric field of quadrupole geometry

$$\vec{E}(r) \sim r^{-4}$$

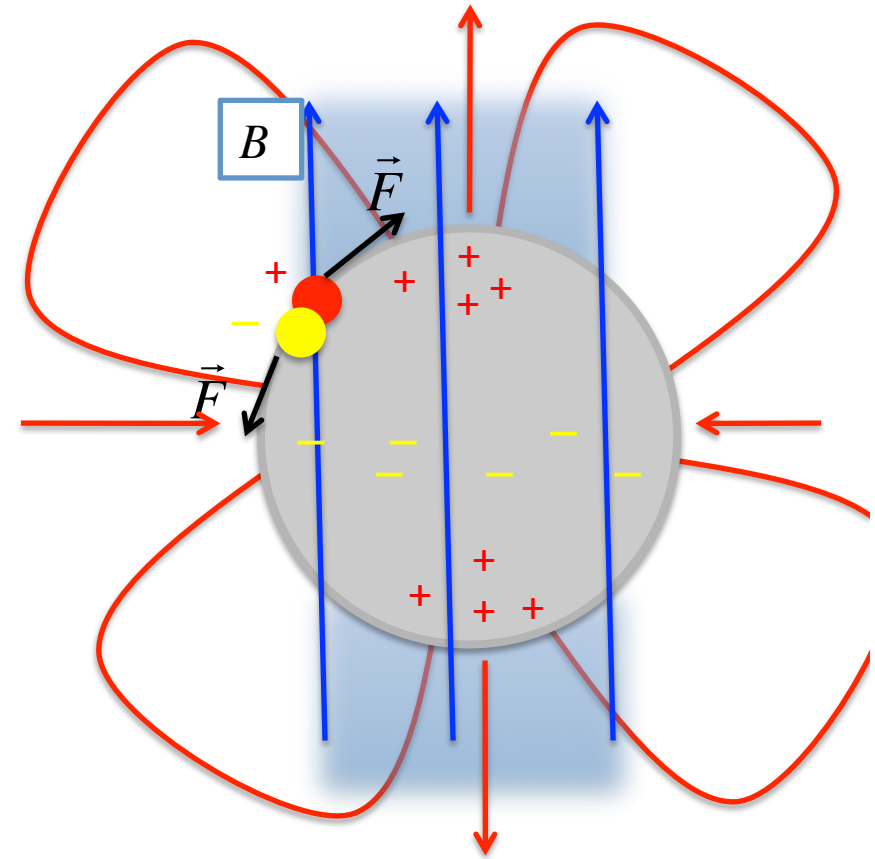
Large scale electric field accelerates particles in the north and south polar caps

$$|\vec{E}_{||}| \sim RB / P$$

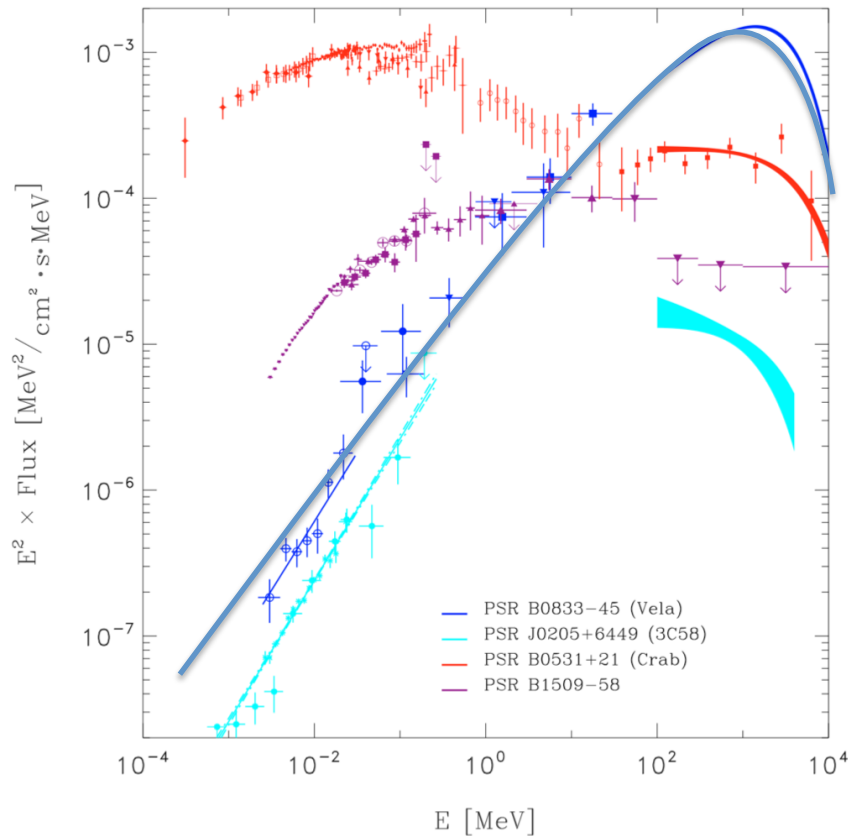
Maximal particle energies

$$E_{\max} \sim e |\vec{E}_{||}| R \sim eR^2 B / P$$

$$\approx 10^{16} \left[\frac{P}{33 \text{ ms}} \right]^{-1} \left[\frac{B}{10^{12} \text{ G}} \right] \text{ eV}$$



Pulsars as particle accelerators



Particle acceleration is accompanied by radiation.

This could not be synchrotron radiation, because the synchrotron cooling time is extremely short

$$t_{synch} \approx 10^{-16} \left[\frac{B}{10^{12} \text{ G}} \right]^{-2} \left[\frac{E_e}{10^6 \text{ eV}} \right]^{-1} \text{ s}$$

The only possibility how particles could be accelerated is if they move along magnetic field lines.

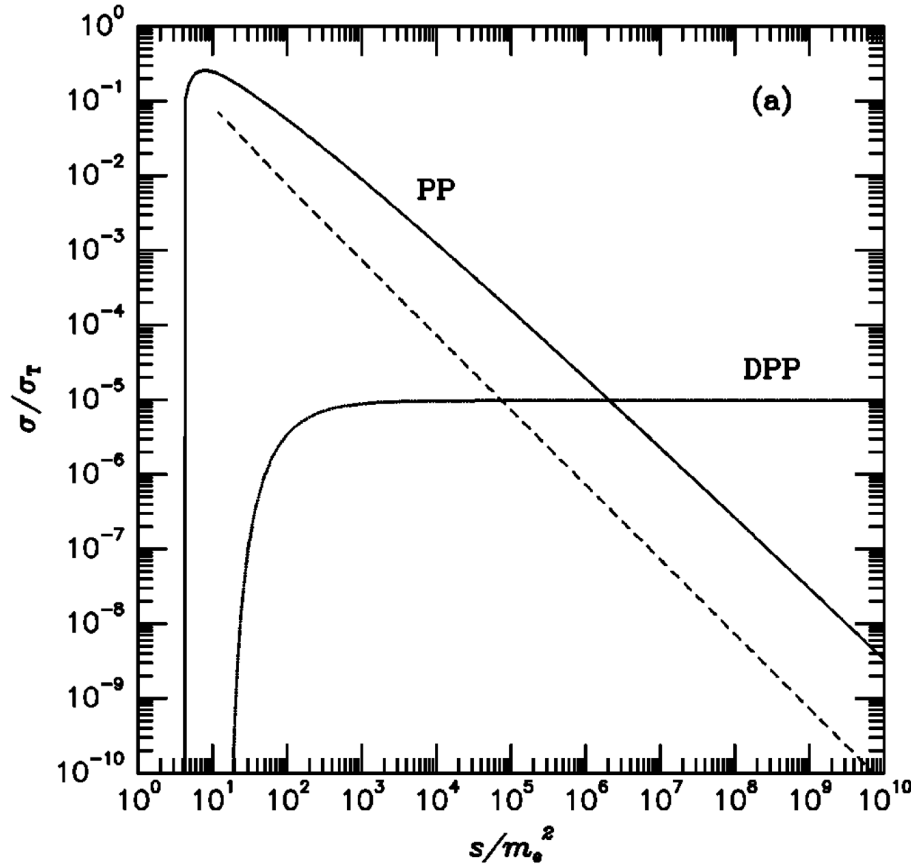
The magnetic field lines are curved. Minimal energy loss for the high-energy electrons is via curvature radiation

$$\omega_{curv} \sim \frac{E^3}{R_{Curv} m^3} \approx 2 \left[\frac{R_{Curv}}{R_{NS}} \right]^{-1} \left[\frac{E_e}{3 \text{ TeV}} \right]^3 \text{ GeV}$$

Particles are accelerated close to the neutron star at least to TeV energy scale.

Interactions of high-energy photons

(remnant from Lecture 2)



Similar process is pair production in photon – magnetic field interaction.

Gamma-rays could produce pairs in collisions with other photons if the CM energy is above two times electron rest energy

$$E_{\gamma 1} \geq \frac{m_e^2}{E_{\gamma 2}}$$

The cross-section of pair production peaks at $\sigma_{\gamma\gamma} \approx 10^{-25} \text{ cm}^2$ and drops as $E^{-1} \ln(E)$ at higher energies. Mean free path of gamma-rays through photon background is

$$\lambda_{\gamma\gamma} = \frac{1}{\sigma_{\gamma\gamma} n_{ph}} \approx 10^4 \left[\frac{n_{ph}}{10^{21} \text{ cm}^{-3}} \right]^{-1} \text{ cm}$$

Number density of keV X-ray photons close to the neutron star is

$$n_x = F \left(\frac{D}{R} \right)^2 \approx 10^{27} \left[\frac{D}{2 \text{ kpc}} \right]^2 \left[\frac{R}{10^8 \text{ cm}} \right]^{-2} \text{ cm}^{-3}$$

Gamma-rays with energies in the GeV range could hardly get out of the emission region near Crab pulsar, because of the pair production.

Pulsar magnetosphere

Curvature radiation quanta produce pairs in interactions with magnetic field and X-ray photons.

The space around the neutron star gets filled with e^+e^- plasma which screens the initial accelerating magnetic field. e^+e^- plasma forms a "**magnetosphere**" around the neutron star.

"Problem of discharge..."

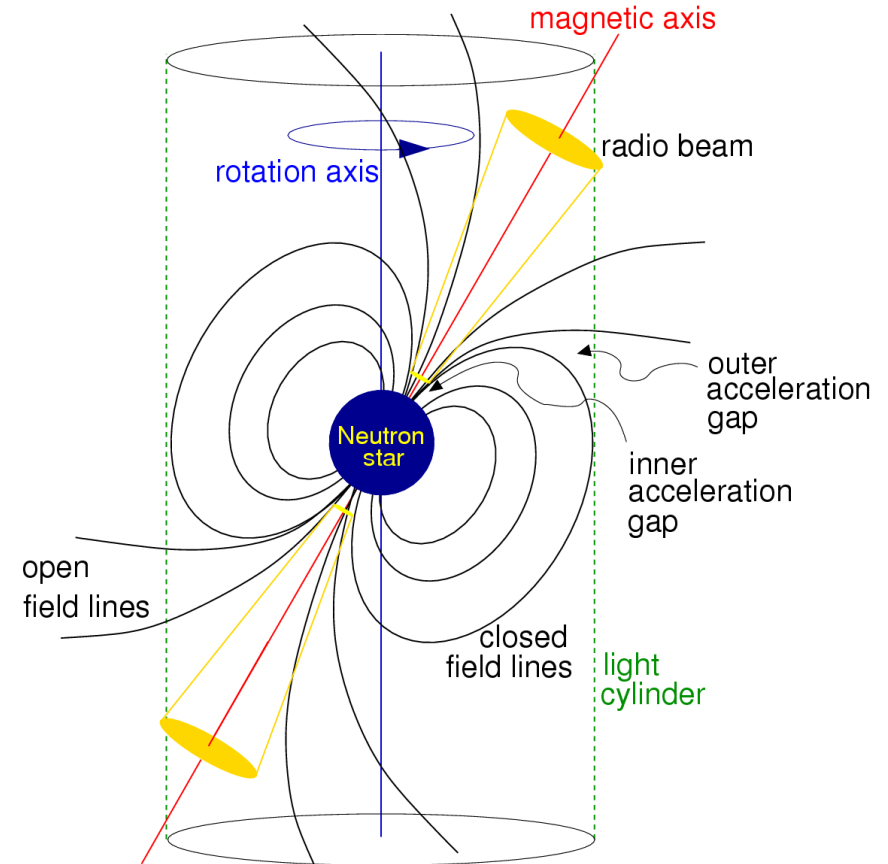
A first estimate of the charge number density in the magnetosphere is found from the condition for the discharge

$$n_{GJ} \approx \frac{\mathcal{E}}{eR} \approx \frac{B}{eP} \approx 10^{13} \left[\frac{B}{10^{12} \text{ G}} \right] \left[\frac{P}{1 \text{ ms}} \right]^{-1} \text{ cm}^{-3}$$

It is called Goldreich-Julian density.

Charges are moving freely along magnetic field lines and gradually escape from the magnetosphere along **open field lines** crossing the **light cylinder** at the distance

$$R_{LC} = \frac{P}{2\pi} \approx 10^8 \left[\frac{P}{33 \text{ ms}} \right] \text{ cm}$$

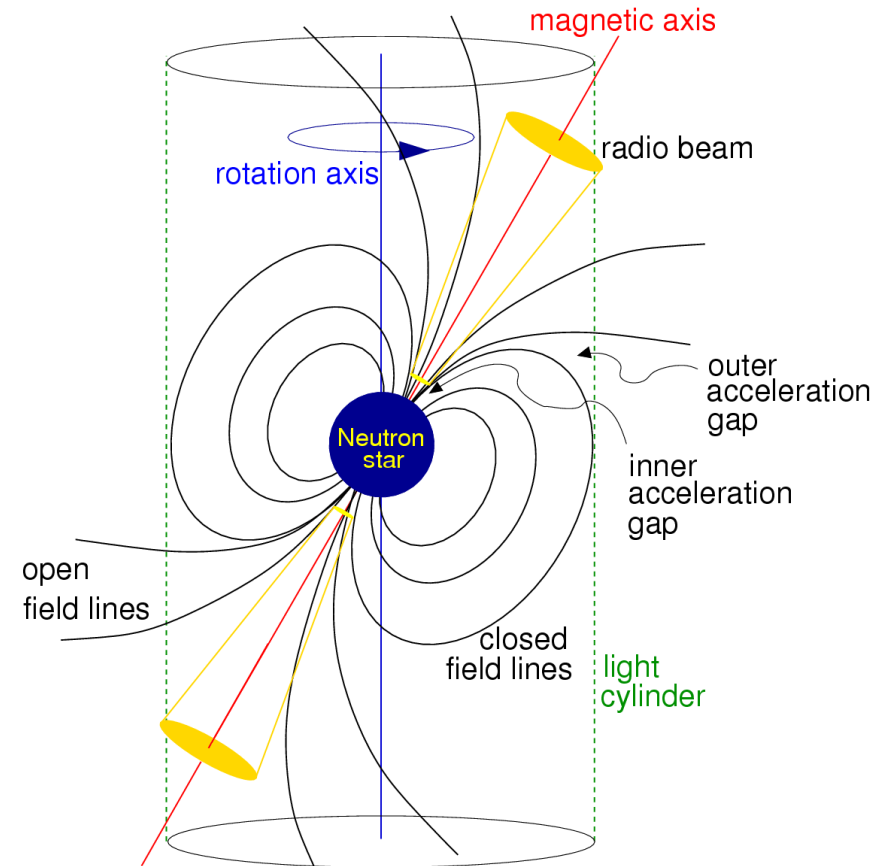


Acceleration gaps in the magnetosphere

Charges are moving freely along magnetic field lines and gradually escape from the magnetosphere along **open field lines** crossing the **light cylinder**.

Vacuum “**acceleration gaps**” form in the polar cap regions (footprints of open field lines) and along the boundary of the close field line region.

Size of the acceleration gaps is “self-regulated” in such a way that they operate at the limit of the discharge.



Pulsar wind

Continuous acceleration and wash out of charged particles from the interior of the light cylinder along the open field lines leads to generation of relativistic particle outflow.

Particle flow also creates currents which generates electromagnetic fields

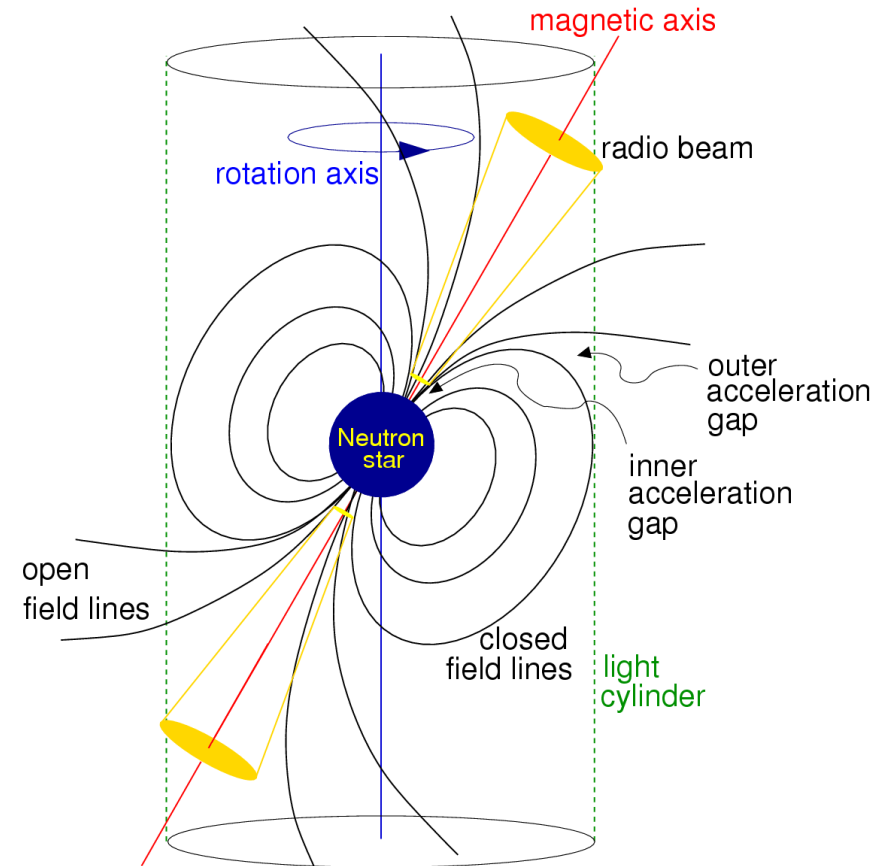
$$B_{GJ} \sim \frac{n_{GJ} R_{LC}^2}{R_{LC}} \sim \frac{B_{LC} R_{LC}}{P}$$

and carry the Poynting flux with the total power

$$\dot{E}_{em} \sim \frac{B^2}{4\pi} \cdot 4\pi R_{LC}^2 \sim \frac{BR^6}{P^4}$$

comparable to the power of magnetic dipole radiation.

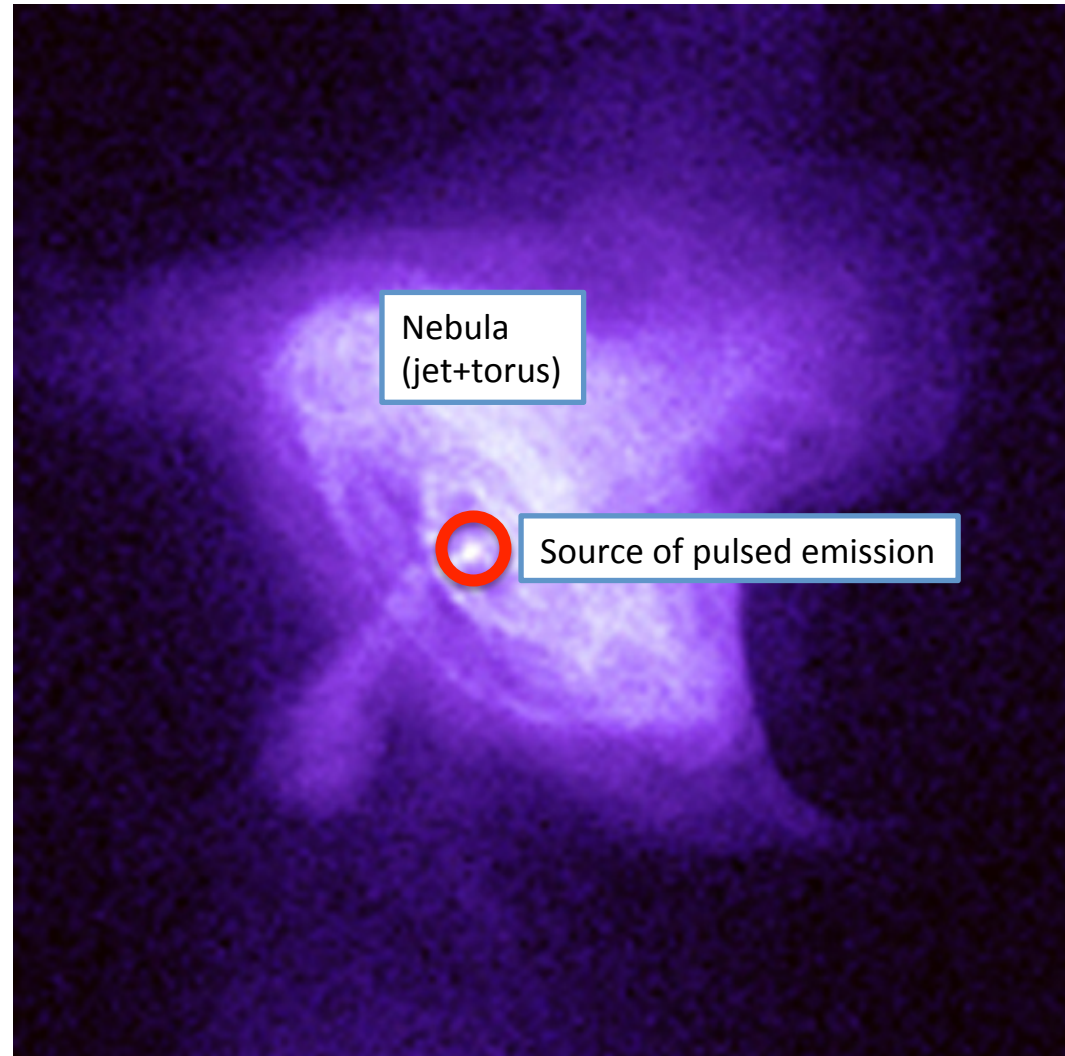
Significant fraction of the pulsar spin-down energy loss rate goes into generation of magnetized relativistic **pulsar wind**.



Pulsar wind nebula

X-ray telescopes resolve Crab into a point source of pulsed emission surrounded by an extended nebula.

Angular size of several arcsecond at the distance ~ 2 kpc corresponds to $\sim 10^{17}$ – 10^{18} cm, i.e. way larger than the size of the light cylinder.



Pulsar wind nebula

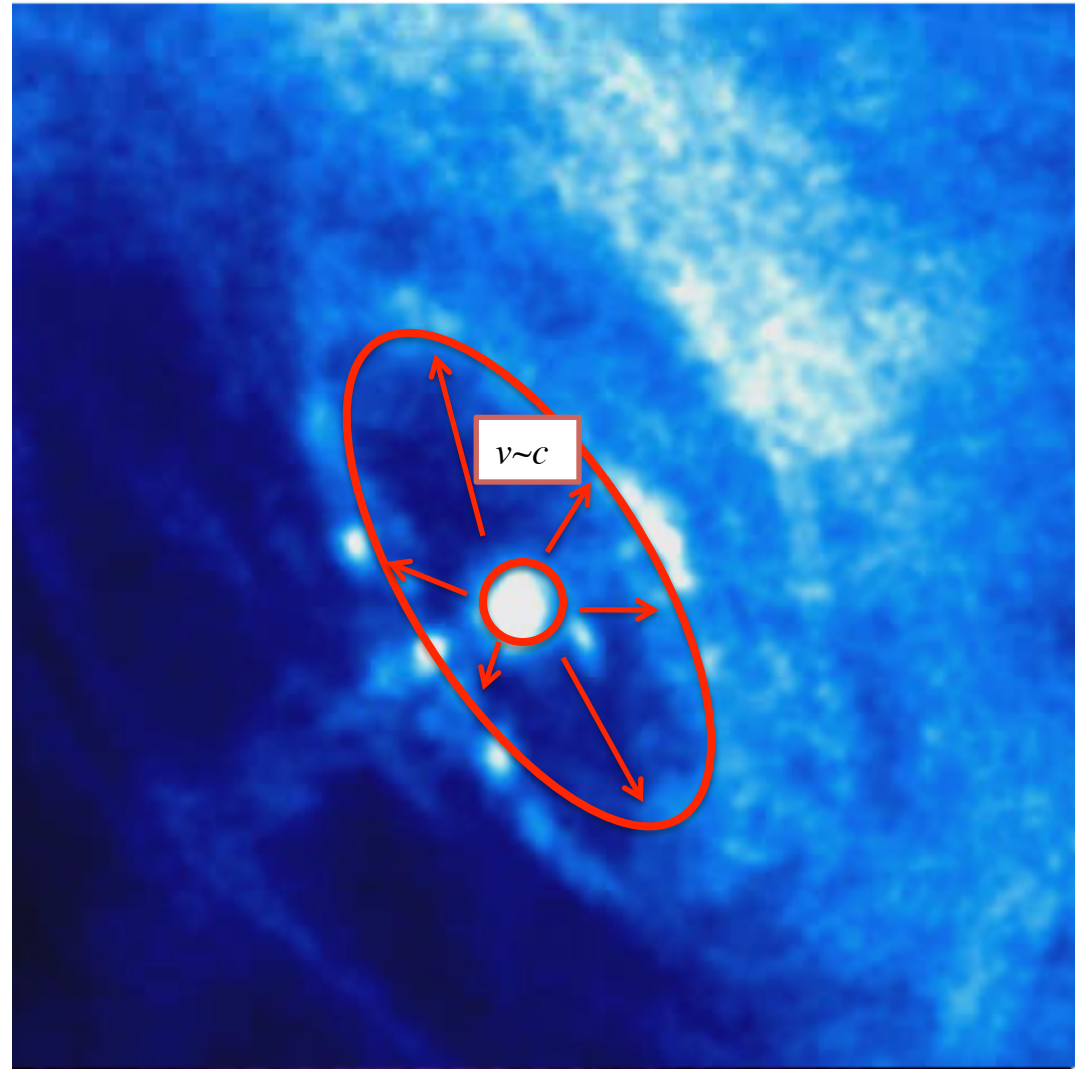
X-ray telescopes resolve Crab into a point source of pulsed emission surrounded by an extended nebula.

Angular size of several arcsecond at the distance ~ 2 kpc corresponds to $\sim 10^{17}$ – 10^{18} cm, i.e. way larger than the size of the light cylinder.

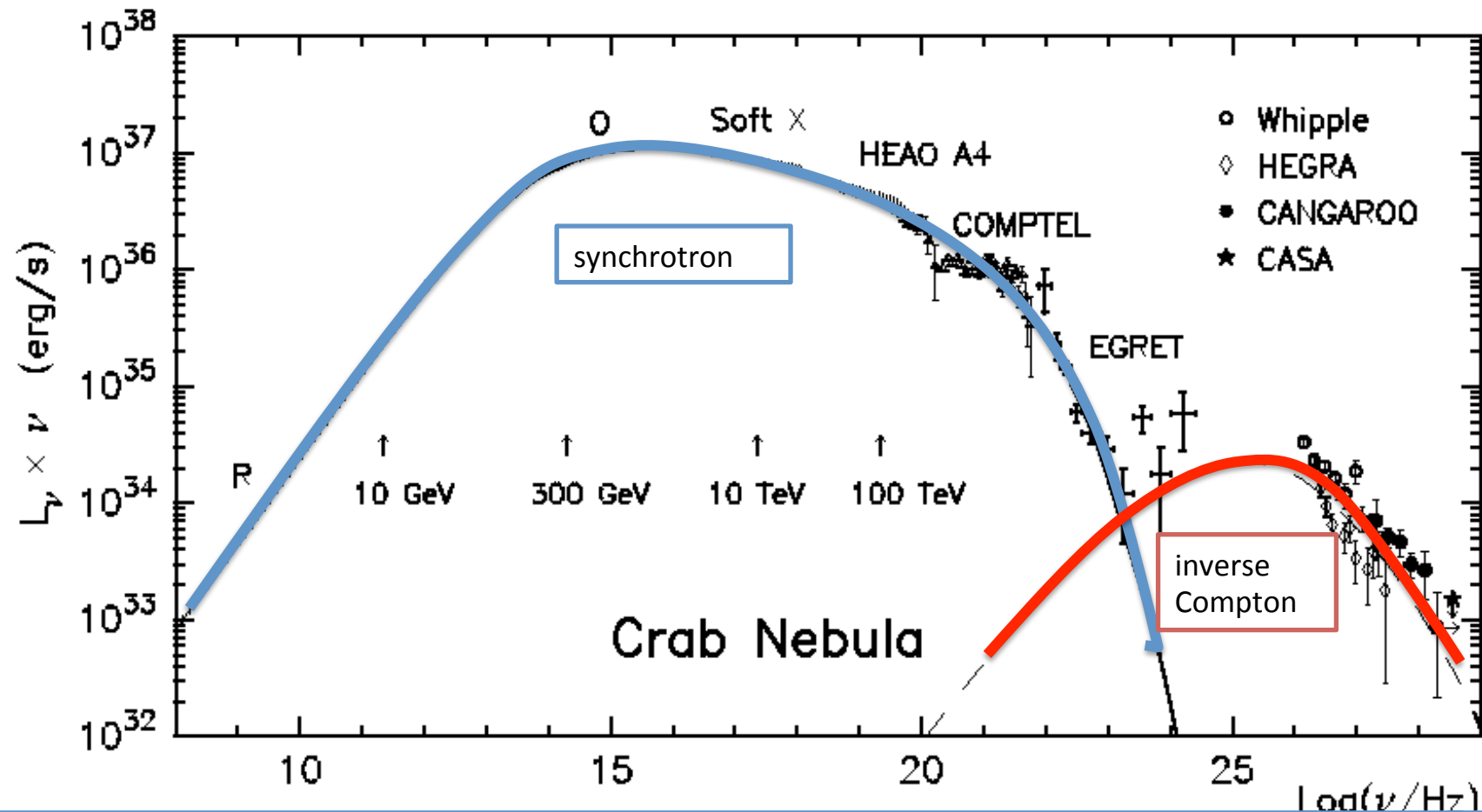
Nebula emission is variable on the time scale of several months ($\sim 3 \times 10^6$ s)

$$t \sim \frac{R}{c} = \frac{10^{17} \text{ cm}}{3 \times 10^{10} \text{ s}} \sim 3 \times 10^6 \text{ s}$$

Central source of pulsed emission generates relativistic outflow feeding the nebula. The outflow is stopped at the termination shock at the distance $\sim 10^{17}$ – 10^{18} cm.



Particle acceleration in the nebula



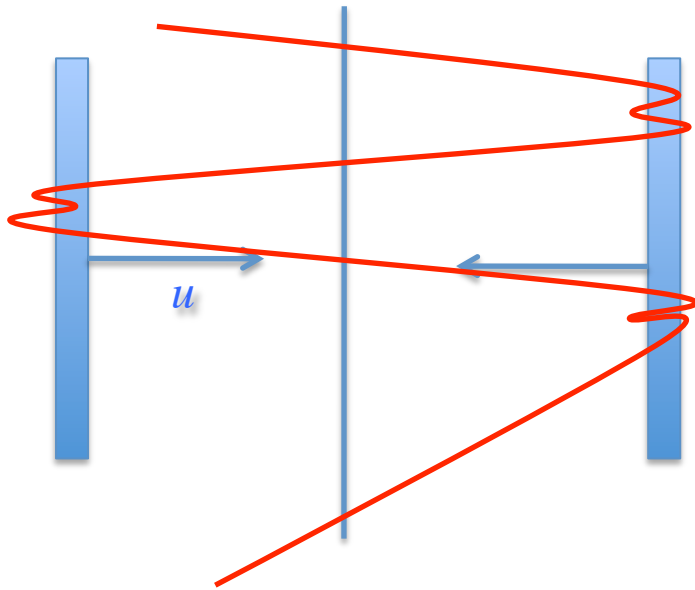
Magnetic field at the shock location could be estimated as

$$B_{PWN} \sim \left(\frac{R_{LC}}{R_{shock}} \right) B_{LC} \sim \left(\frac{R_{LC}}{R_{shock}} \right) \left(\frac{R}{R_{LC}} \right)^3 B \sim 10^{-4} \text{ G}$$

Synchrotron radiation in the GeV energy range is produced by multi-PeV electrons:

$$\omega \approx 0.5 \left[\frac{B}{10^{-4} \text{ G}} \right] \left[\frac{E}{10^{16} \text{ eV}} \right]^2 \text{ GeV}$$

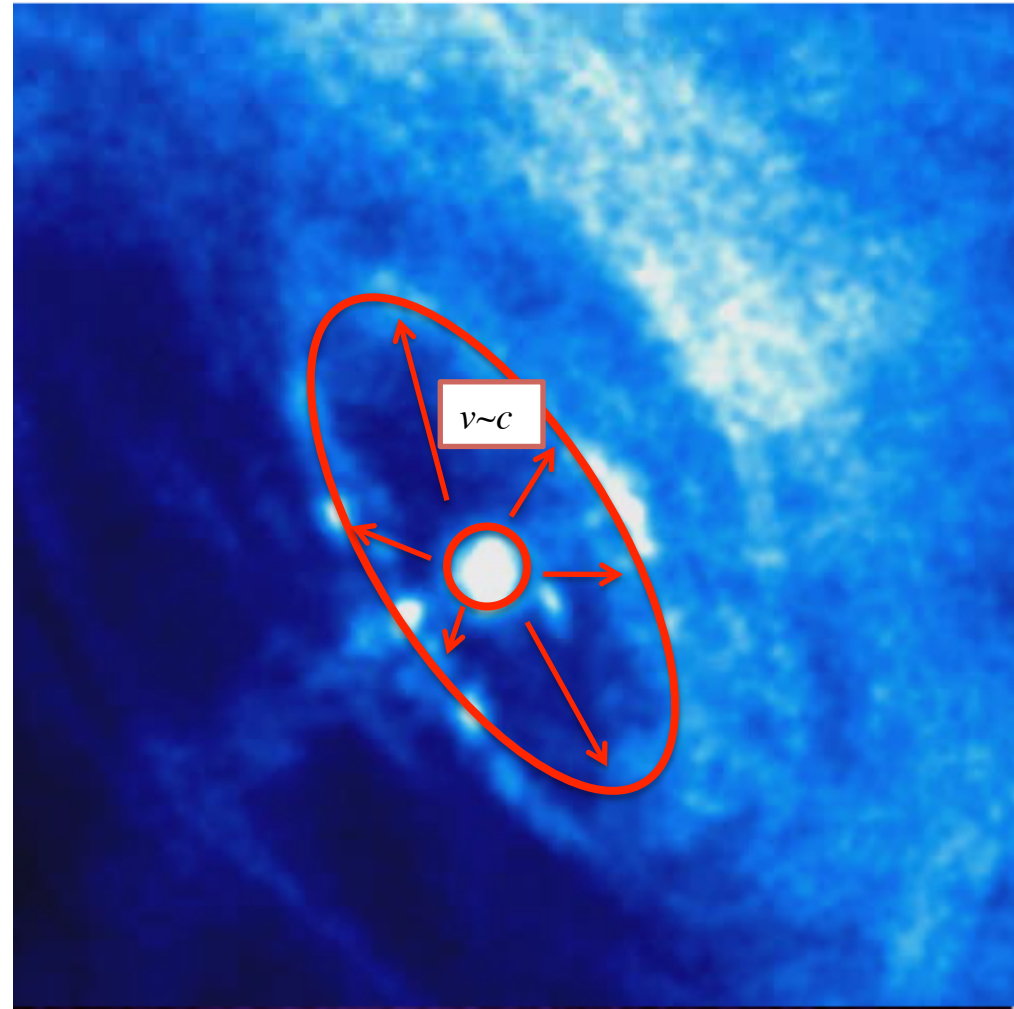
Particle acceleration in the nebula



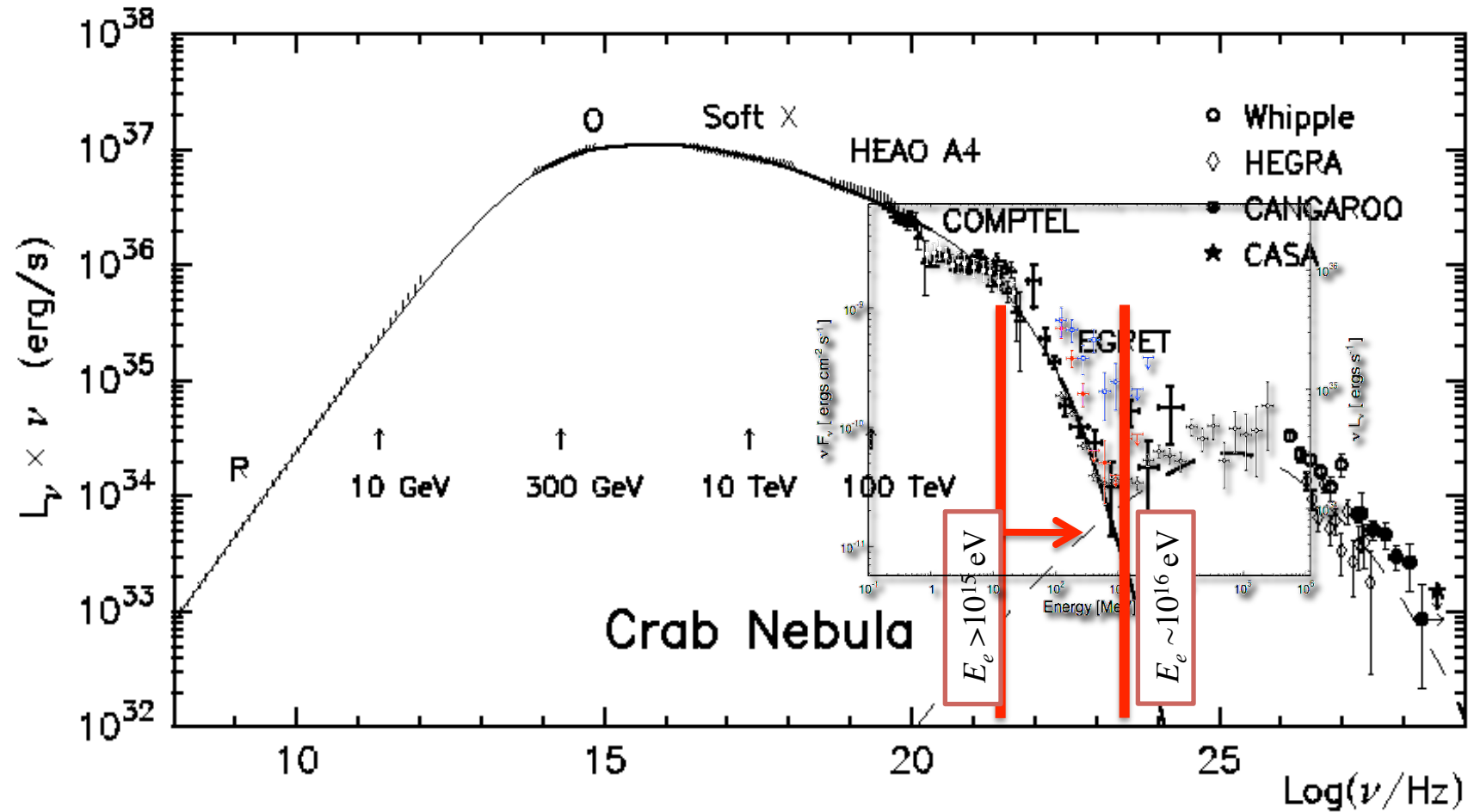
Relativistic pulsar wind is stopped by the interstellar medium. A shock is formed at the pulsar wind / ISM interface.

Relativistic shock operates as efficient particle accelerator

$$E_{max} \approx 3 \times 10^{16} \left[\frac{B}{10^{-4} \text{ G}} \right] \left[\frac{R}{10^{18} \text{ cm}} \right] \text{ eV}$$



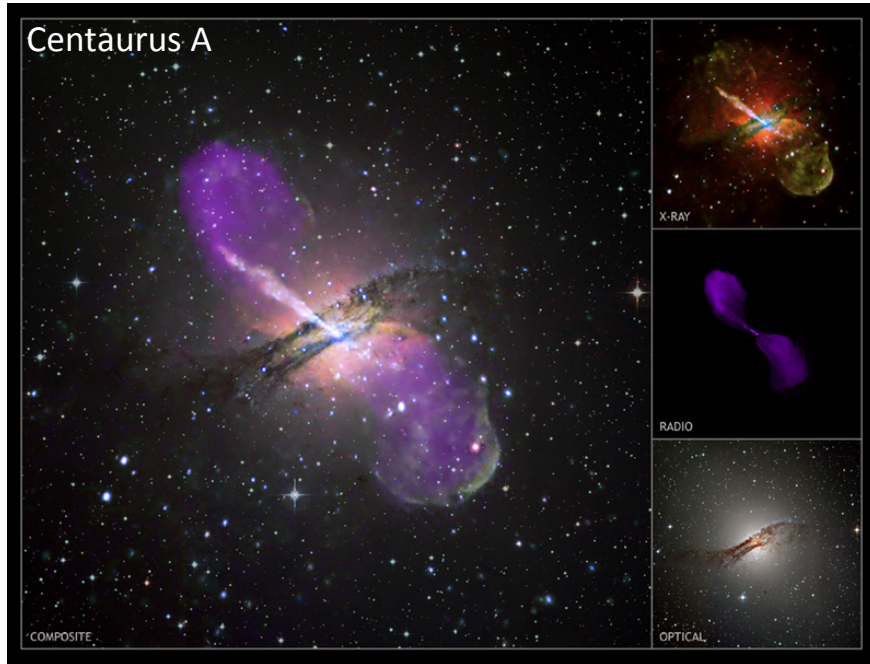
Particle acceleration in the nebula



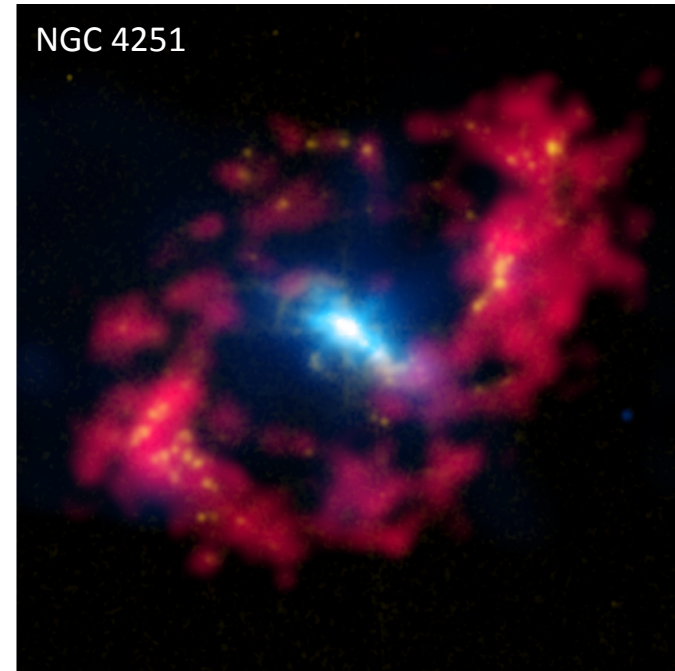
Two γ -ray telescopes, Fermi and AGILE, detect flares from Crab at the energies up to 1 GeV, on a time scale ~ 1 day. This indicates that acceleration takes place on the time scale about the light crossing time of a (fraction of) the termination shock of the pulsar wind.

Active Galactic Nuclei

Active Galactic Nuclei



Radio loud (radio galaxies, quasars, blazars)



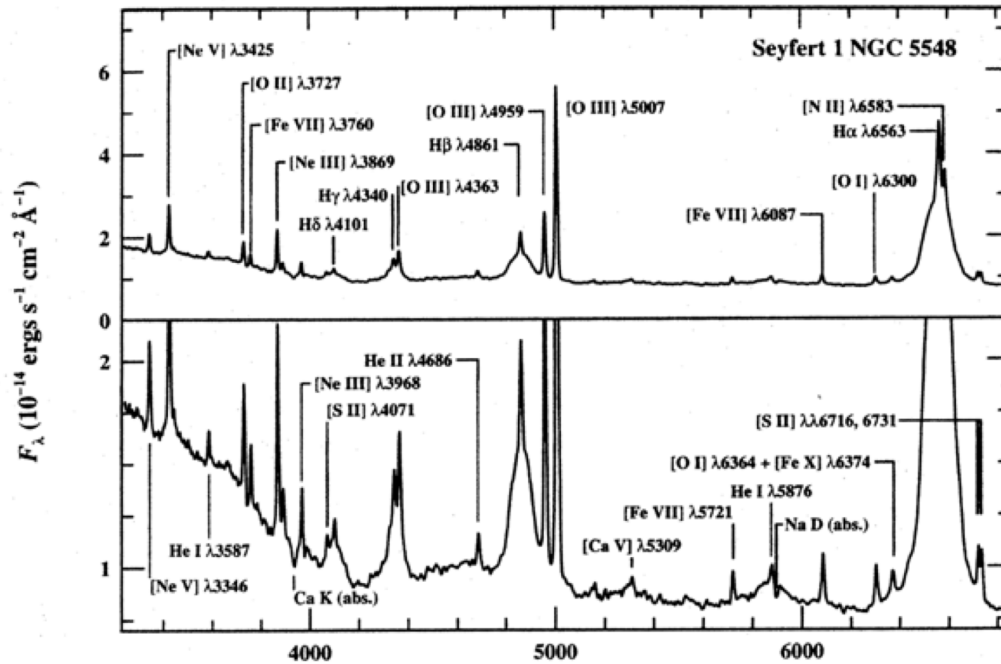
Radio quiet (Seyfert galaxies and quasars)

Powerful emission $L \sim L_{Edd} \approx 10^{45} \left[\frac{M}{10^7 M_{\odot}} \right] \text{ erg/s}$

variable on very short time scale $t_{var} \sim (1-10) \frac{G_N M}{c^3} \sim (1-10) \left[\frac{M}{10^7 M_{\odot}} \right] \text{ hr}$

originates from activity of supermassive black hole

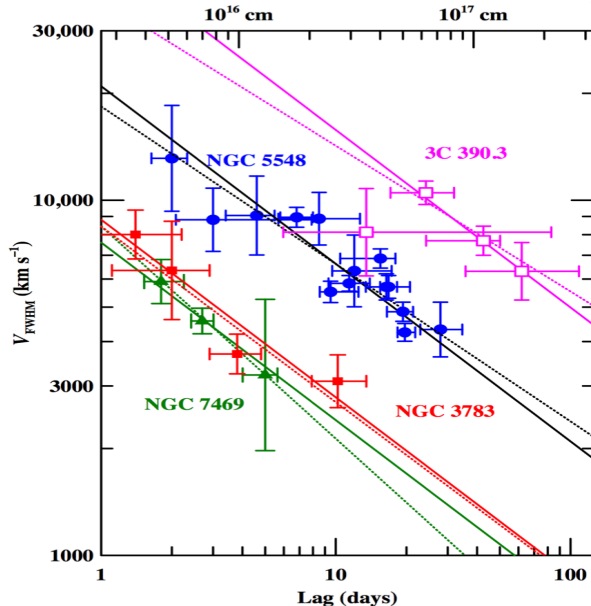
Active Galactic Nuclei



Optical spectra of AGN are characterized by the presence of narrow and broad emission lines

$$\frac{\Delta\lambda}{\lambda} \sim v_K \approx \sqrt{\frac{G_N M}{d}}$$

The “Broad Line Region” is situated at the distances $d \sim 10^4 G_N M$ so that the line widths reach $\sim 10^{-2}$ and in extreme cases ~ 1 .

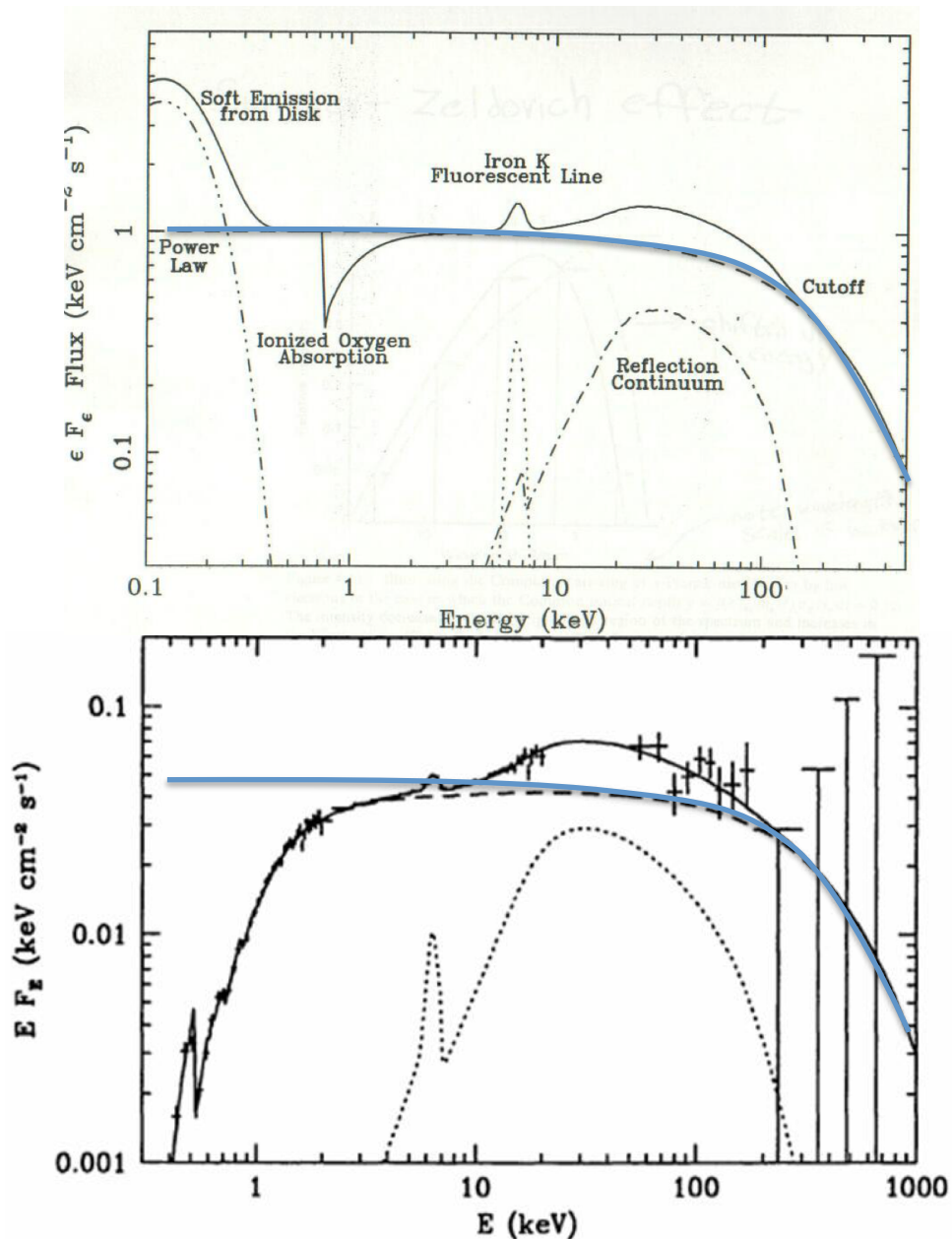


Masses of black holes in the central engines of AGN could be estimated (measured?) through e.g “reverberation mapping” technique. Broad lines are excited by the flux of radiation from the black hole. A flare of the central source has an “echo” in the broad lines after a time delay $\Delta t \sim d/c$.

Measuring Δt one could derive the black hole mass from the relation

$$M \approx \frac{\Delta t \Delta\lambda^2}{G_N \lambda^2}$$

Seyfert galaxies



Seyfert galaxies are (mostly) radio quiet AGN typically found in spiral galaxies.

They do not accelerate particles and their high-energy emission has (most probably) thermal origin.

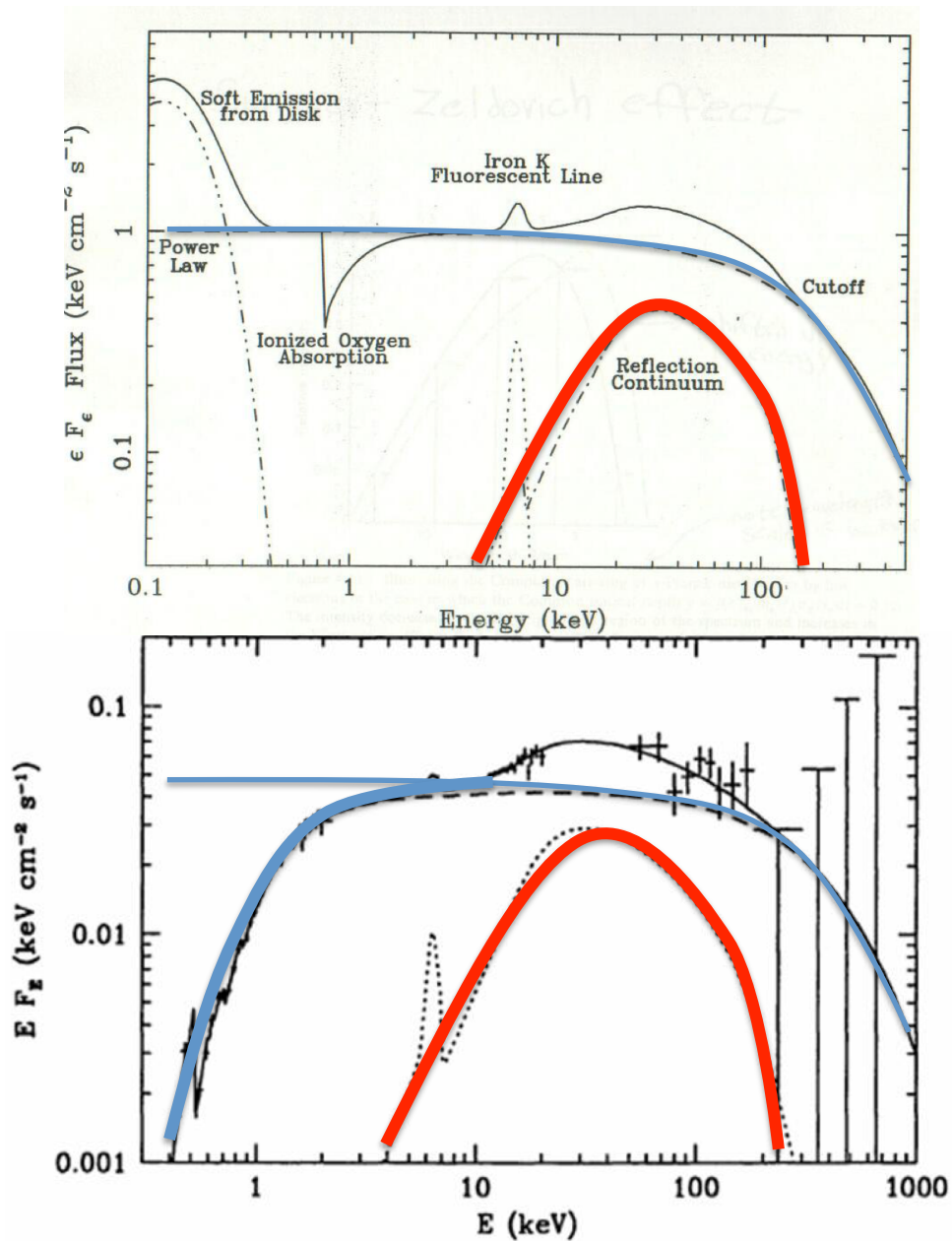
Typical temperature of accretion flow in the Eddington limit is

$$T \approx \left(\frac{G_N M m_p}{\sigma_T R^2} \right)^{1/4} \approx 50 \left[\frac{M}{10^7 M_\odot} \right]^{-1/4} \text{ eV}$$

The spectral feature produced by the accretion flow (accretion disk) is known as “Big Blue Bump”.

The accretion disk is surrounded by a “corona” composed of matter which failed to cool sufficiently to settle into accretion disk. Electrons in this hot corona are mildly relativistic and emit photons at the energies $E \sim 100 \text{ keV}$ via “Comptonisation” process (multiple Compton scattering).

Seyfert galaxies

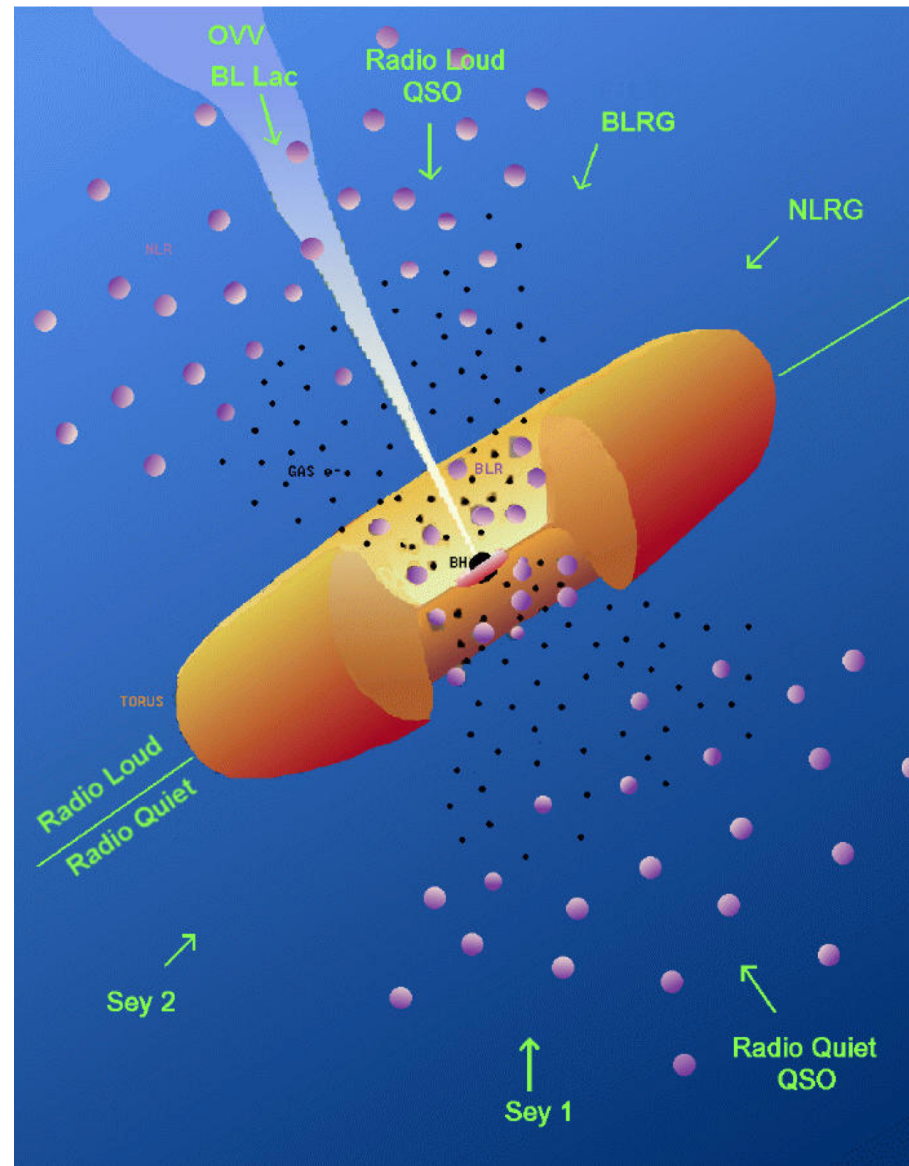


The dense accretion disk reflects part of radiation from the hot corona. This results in production of a “**reflection hump**” at the energy $E \sim 30 \text{ keV}$.

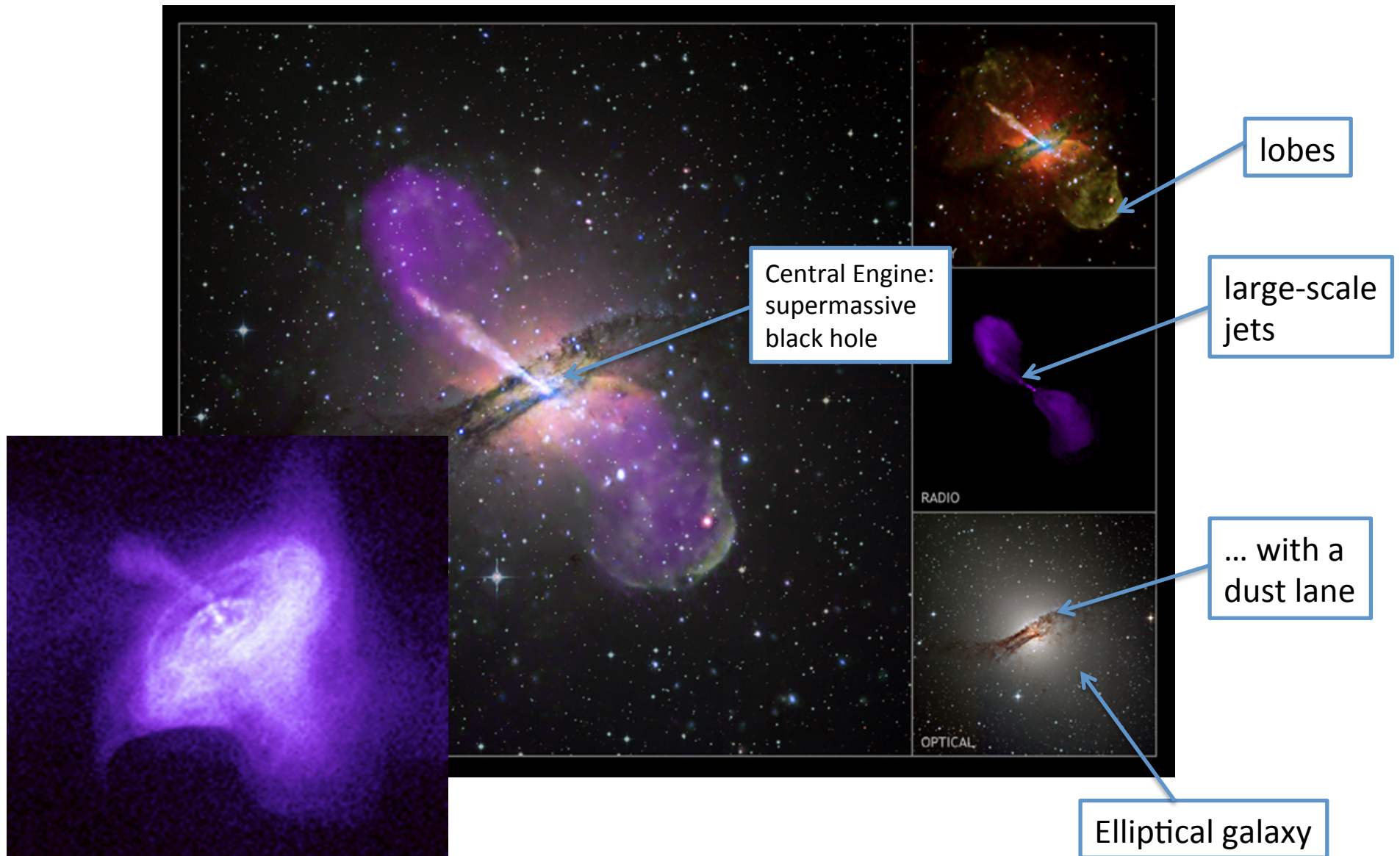
Seyfert galaxies are usually divided into two classes: **Seyfert I** and **Seyfert II**.

Soft X-ray emission from Seyfert II galaxies is suppressed by obscuring material with large column densities $N_{\text{H}} > 10^{23} \text{ cm}^{-2}$. Obscuration also prevents detection of broad emission lines in the visible band.

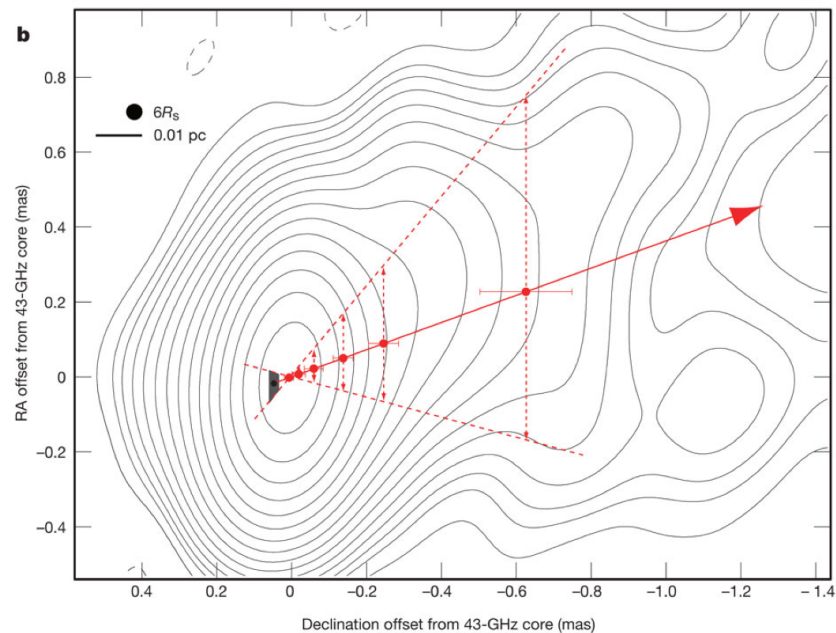
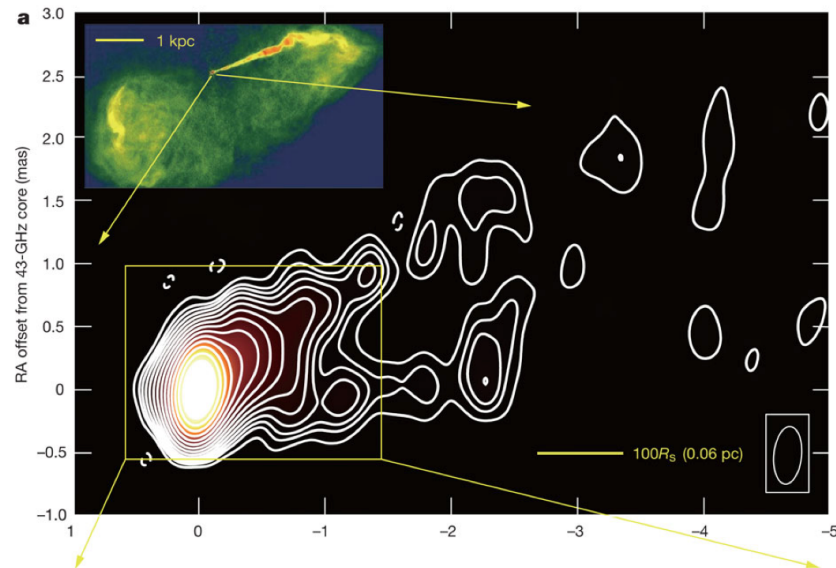
"Unified scheme" of AGN



Radio galaxies



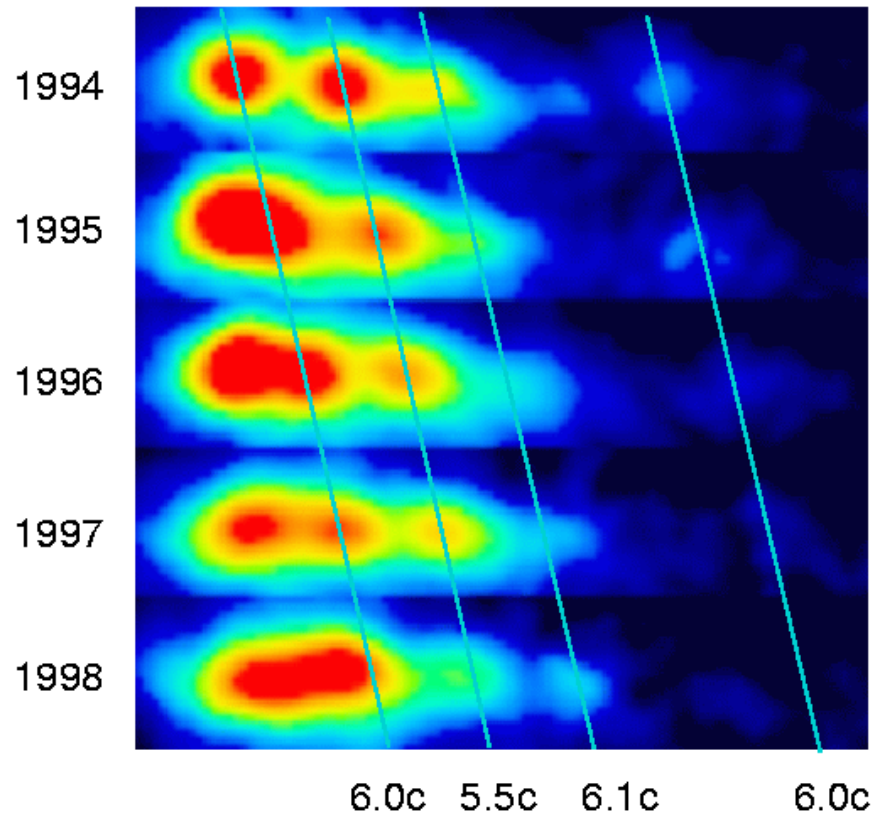
Radio galaxies



Jets of the nearest radio galaxies could be resolved down to the distance scales of $\sim 10-100$ Schwarzschild radii of the supermassive black hole.

At this distance scale they are already well collimated flows. The region of formation of the jet is situated inside this distance scale.

Radio galaxies

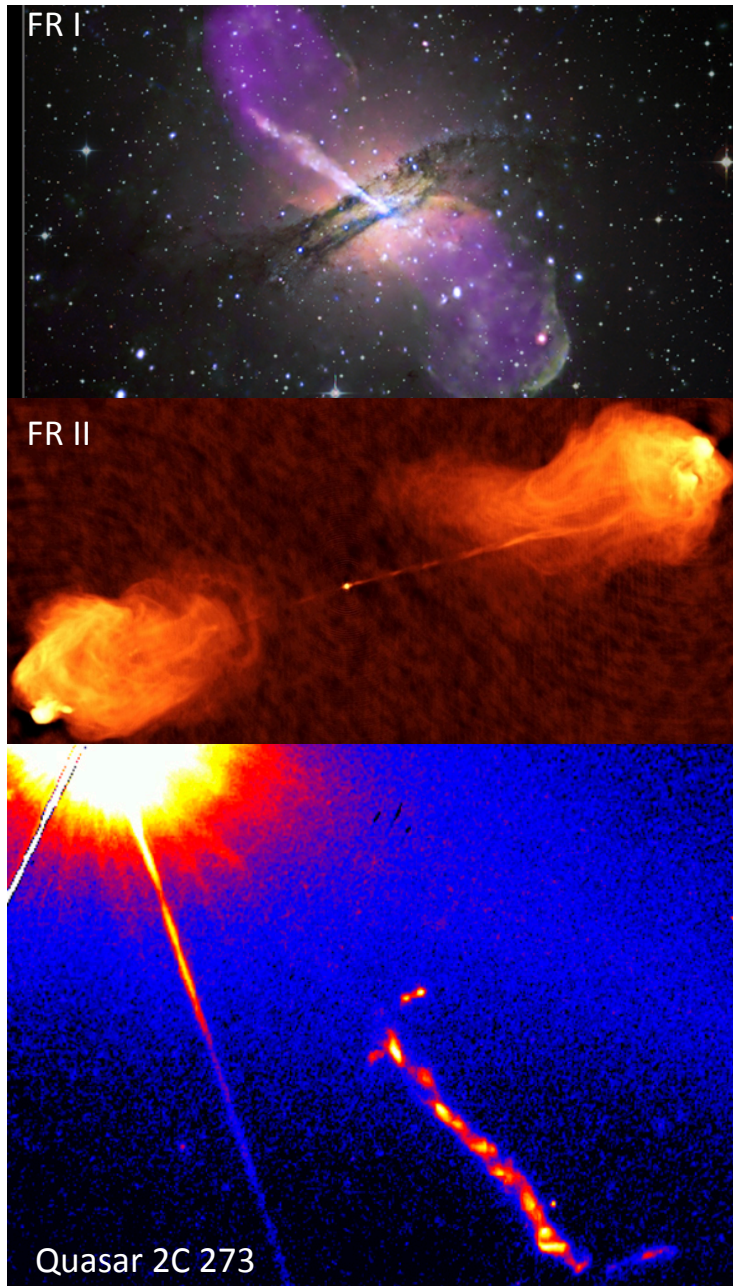


Inhomogeneities in the jets move away from the central engine, sometimes with the apparent superluminal velocity.

$$v_{app} = v \frac{\alpha}{1 - v \cos \alpha}; \quad v_{app,max} \approx 2v\Gamma$$

Observations of $v_{app} \sim 10$ show that inhomogeneities in the jet move with large bulk Lorentz factors $\Gamma \sim 10$

Radio galaxies and quasars



Radio galaxies, similarly to Seyfert galaxies are also divided on two broad classes: **FR I** and **FR 2** (for Fanaroff-Riley).

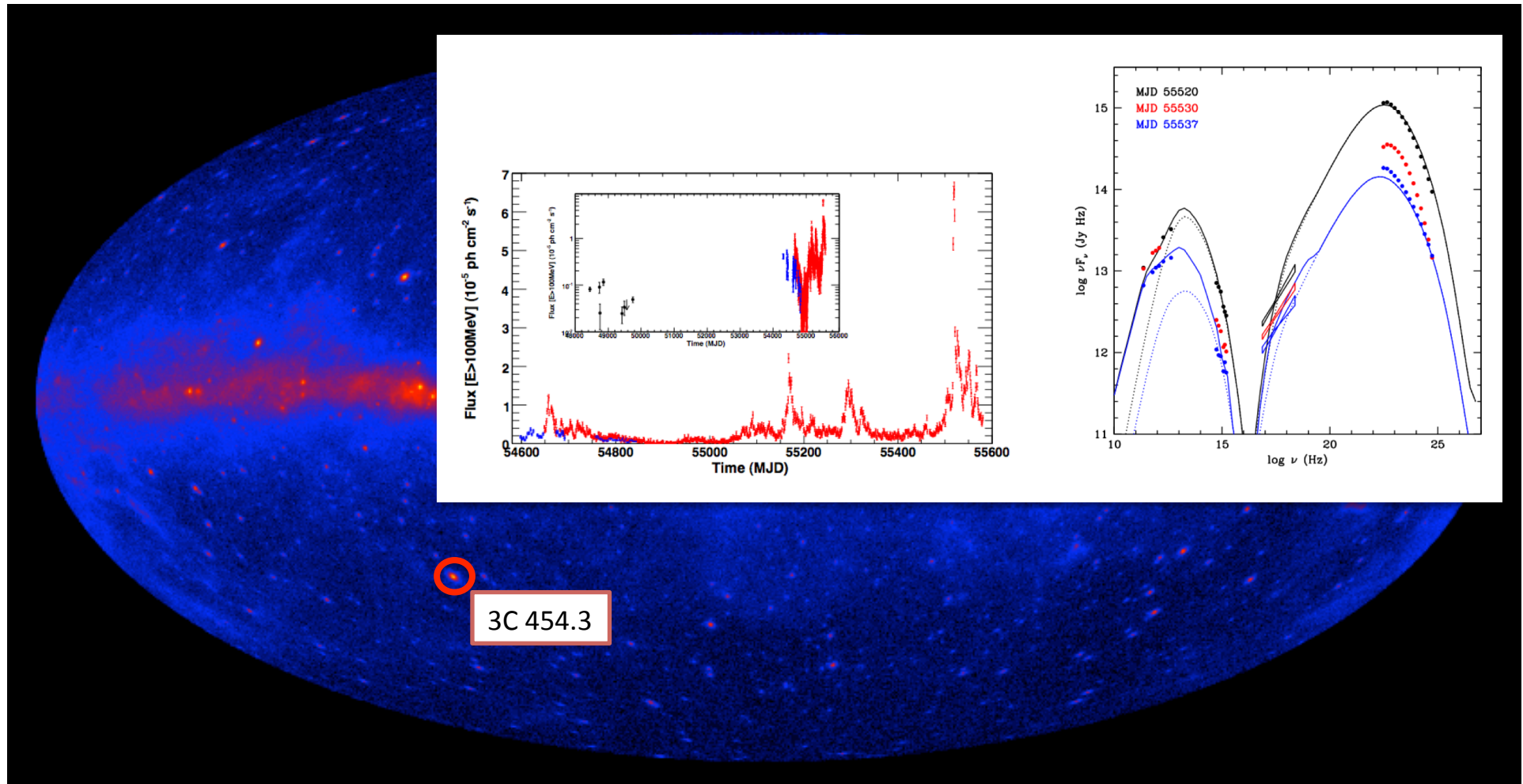
Radio galaxies in the present day Universe are typically operating at luminosities much below the Eddington limit.

Distant ($z \sim 1$) analogues of the radio galaxies, radio loud **quasars** had much higher luminosities, saturating the Eddington limit.

Observational properties of radio galaxies with jets aligned along the line of sight, collectively known as **blazars**, are significantly different from those with the misaligned jets. They are commonly observed in the gamma-ray band.

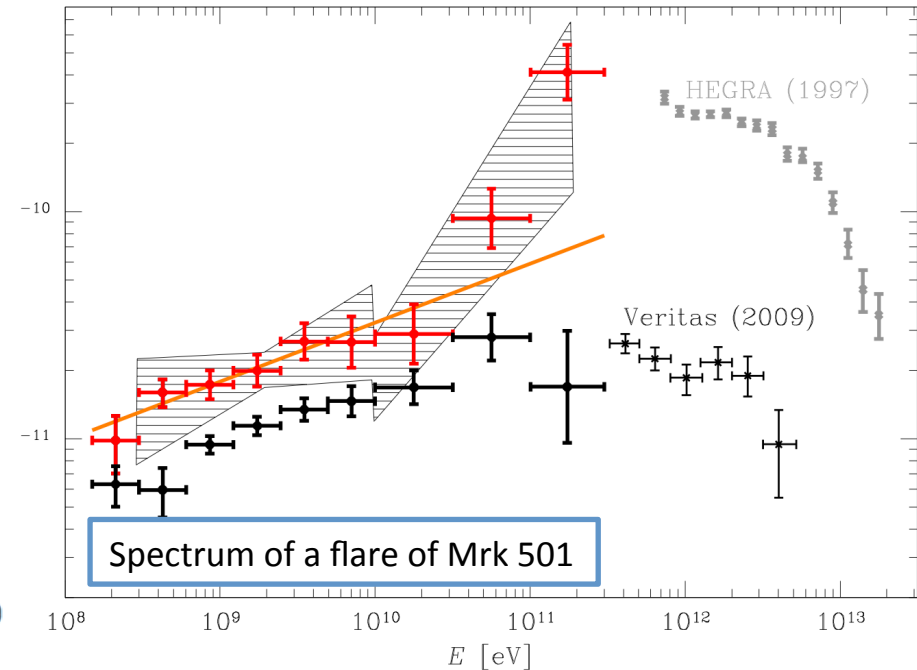
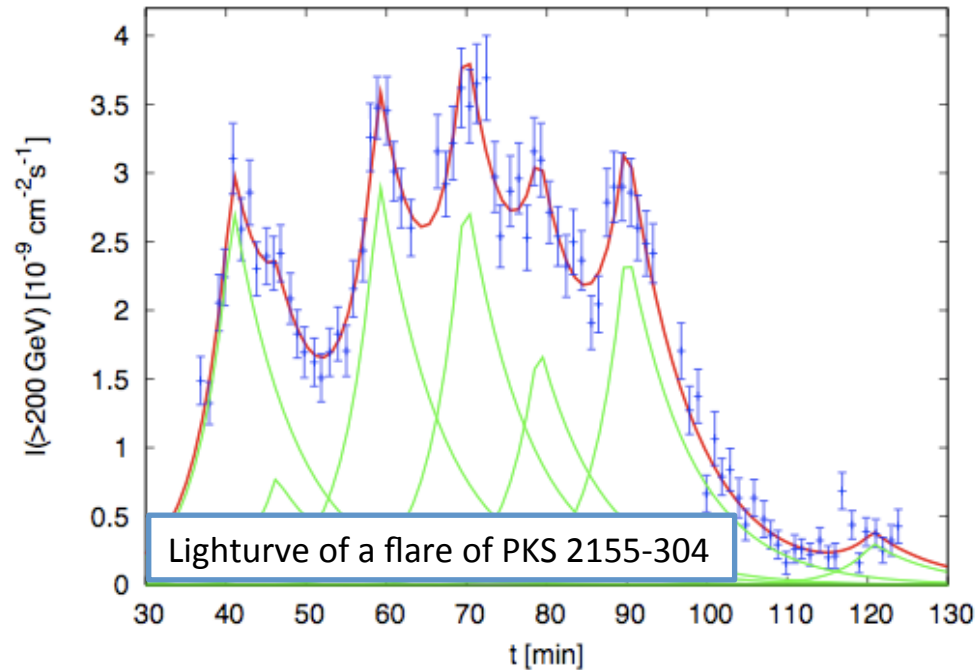
Apparent luminosity of the blazars is enhanced by the Doppler effect $L_{app} \sim \delta^4 L$ where δ is the Doppler factor.

Blazars



Spectra of emission from blazars have characteristic “synchrotron–inverse Compton” two-bump appearance. Both synchrotron and inverse Compton emission are variable on short time scales down to the light crossing time of the supermassive black hole.

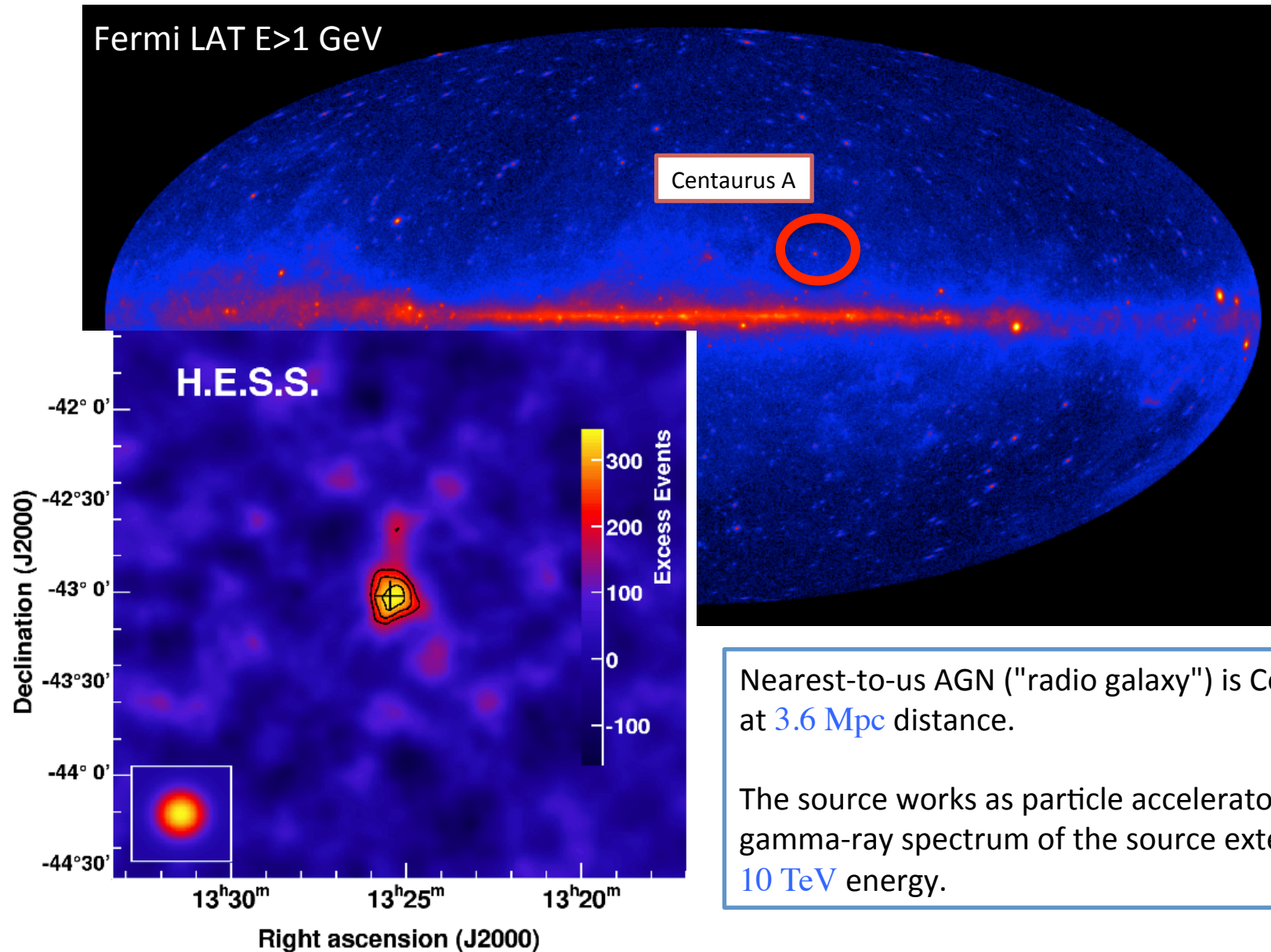
Blazars



Gamma-ray emission from blazars reveals a range of extreme properties, like fast variability on the time scale equal or shorter than the light crossing time of the black hole or peculiar spectral shapes during the flaring activity.

The observed gamma-ray emission comes from the base of the AGN jet from the distance scales at most $d \sim \Gamma^2 R_{BH} \simeq (100 - 1000) R_{BH}$.

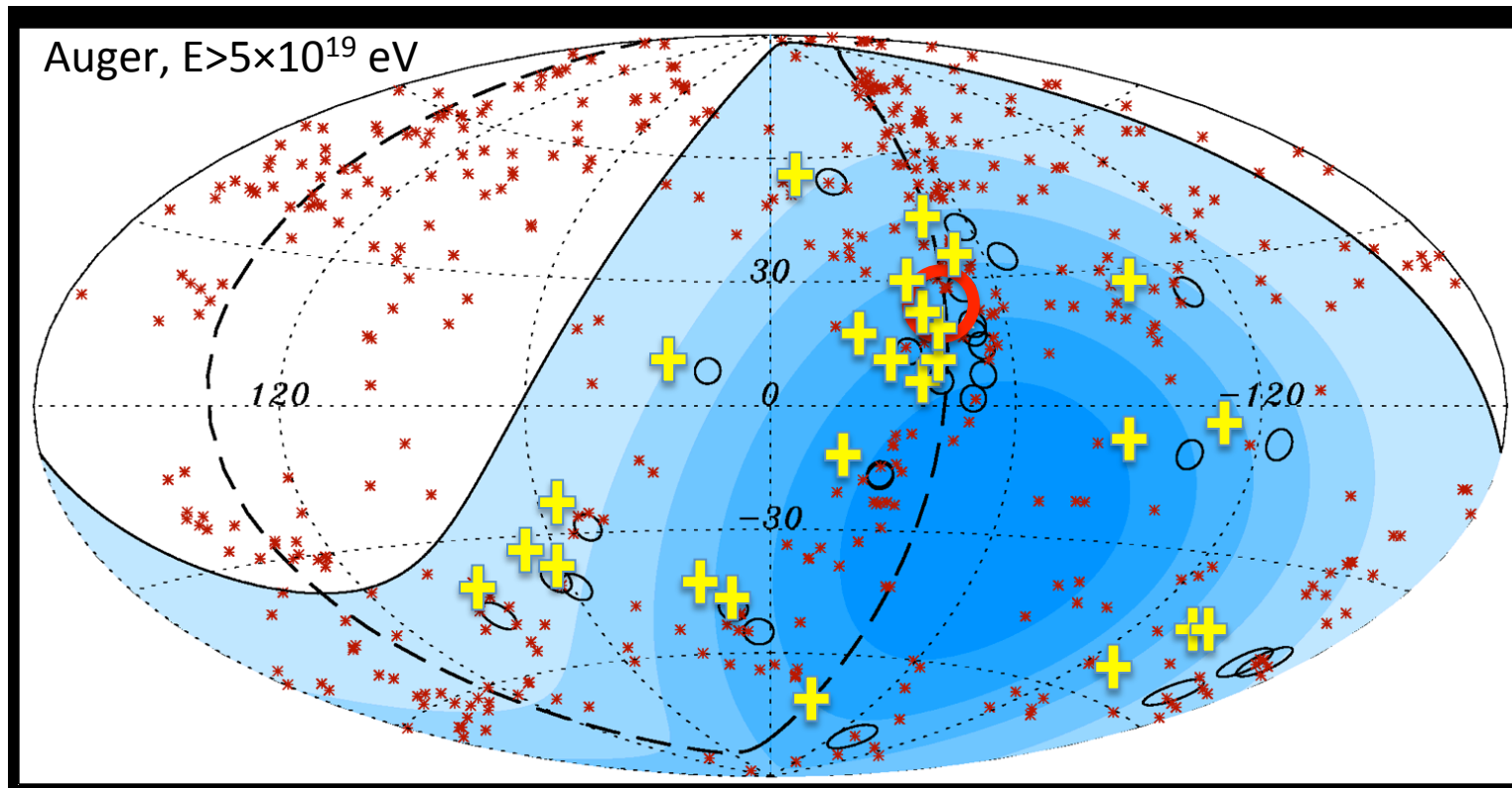
AGN as potential sources of UHECR



Nearest-to-us AGN ("radio galaxy") is Centaurus A at [3.6 Mpc](#) distance.

The source works as particle accelerator. The gamma-ray spectrum of the source extends up to [10 TeV](#) energy.

AGN as potential sources of UHECR



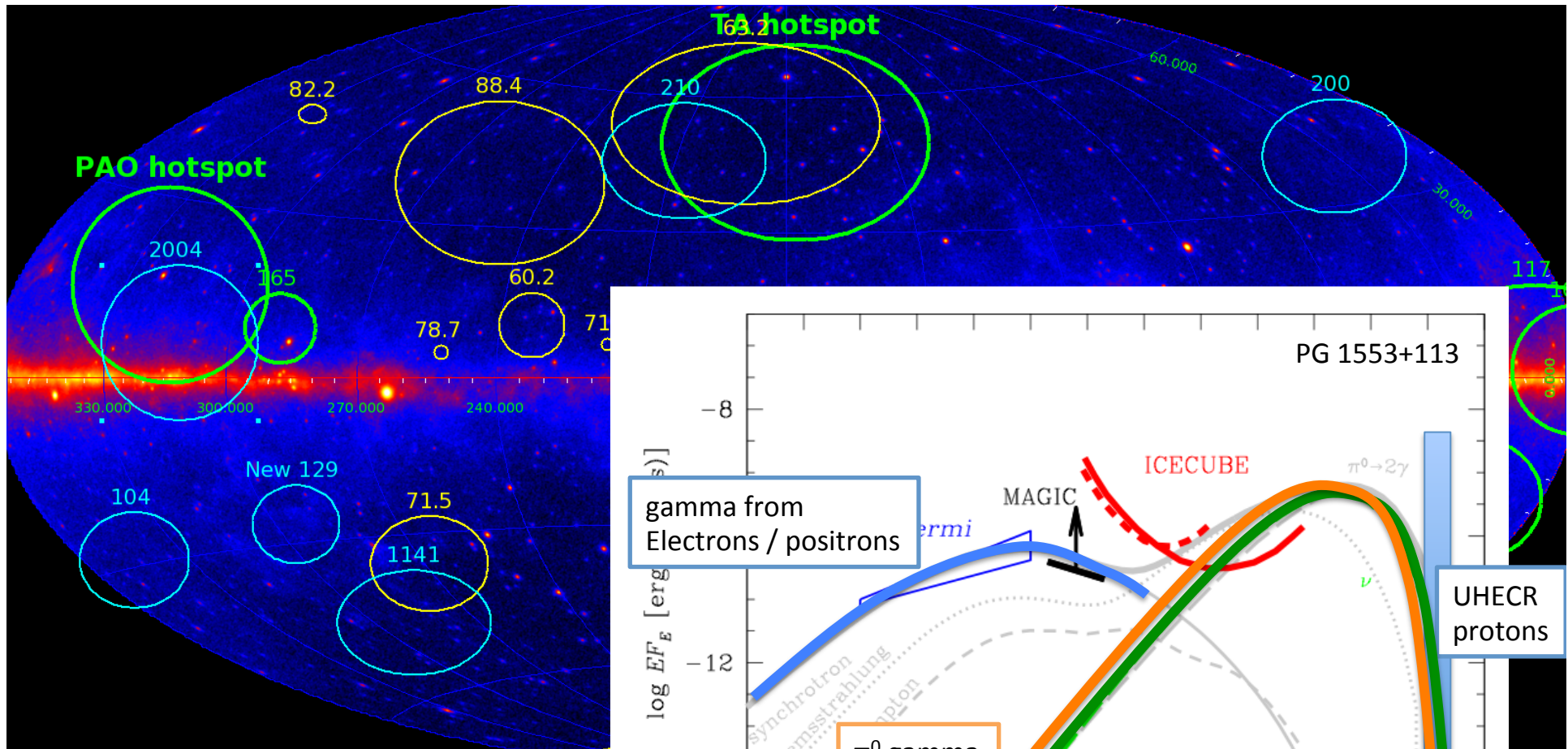
The direction toward Centaurus A is coincident with the direction of an “excess” of UHECR events, within $\sim 20^\circ$ around the source position.

Large angular spread of events around the source could be explained by UHECR deflections in Galactic and extragalactic magnetic fields.

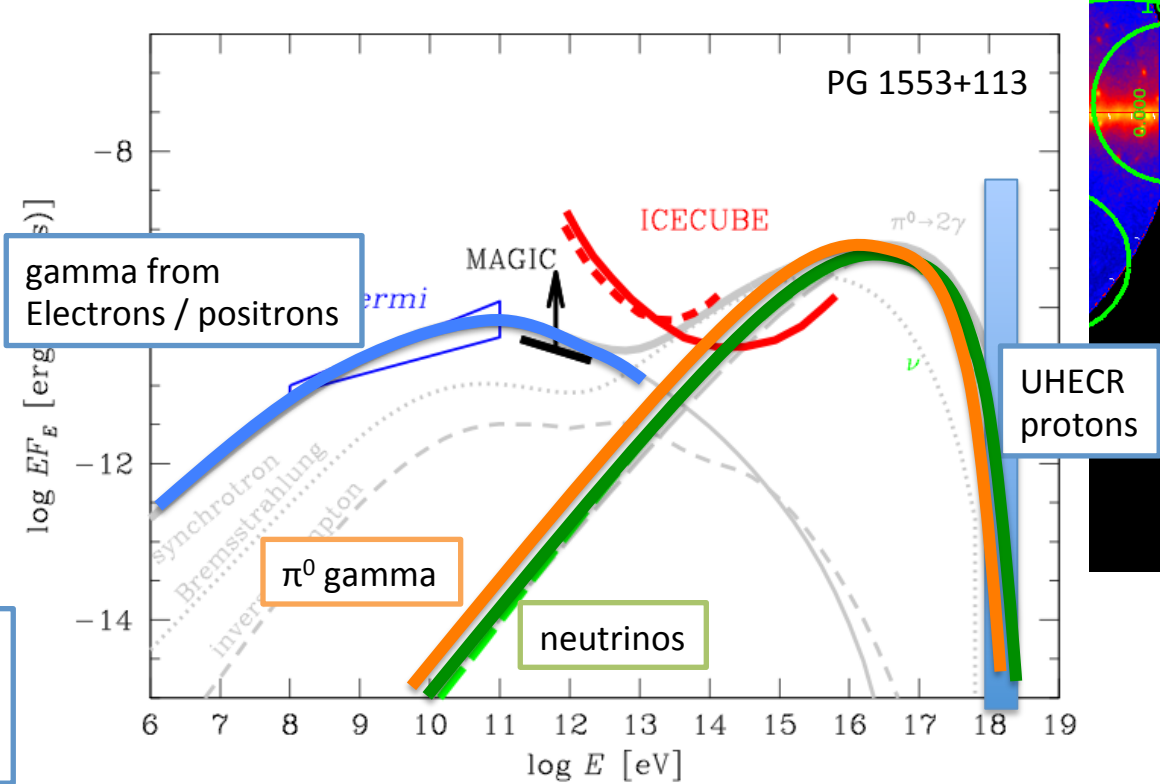
Detection of UHECR from the nearest AGN could provide a useful diagnostics of the efficiency of particle acceleration process in these sources and on the location of the acceleration sites

$$E_{max} \approx 3 \times 10^{19} \left[\frac{B}{10^4 \text{ G}} \right] \left[\frac{R}{10^{13} \text{ cm}} \right] \text{ eV}$$

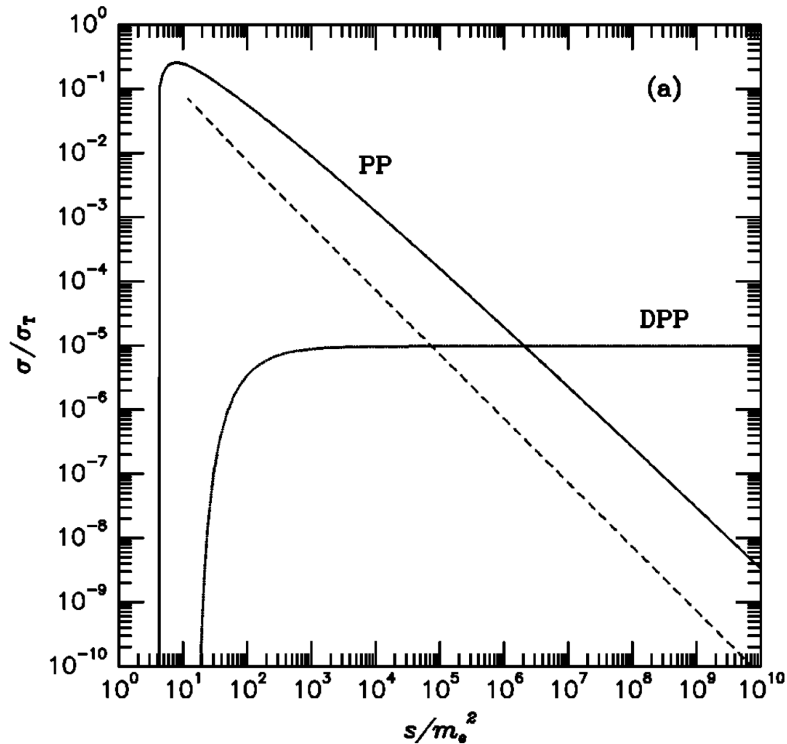
AGN as potential sources of neutrinos



Interactions of high-energy protons lead to production of neutrino and electromagnetic flux



Pair production and electromagnetic cascade



Gamma-rays could produce pairs in collisions with other photons if the CM energy is above two times electron rest energy

$$E_{\gamma 1} \geq \frac{m_e^2}{E_{\gamma 2}} \sim 25 \left[\frac{E_{\gamma 2}}{10 \text{ eV}} \right]^{-1} \text{ GeV}$$

The cross-section of pair production peaks at $\sigma_{\gamma\gamma} \approx 10^{-25} \text{ cm}^2$ and drops as $E^{-1} \ln(E)$ at higher energies. Mean free path of gamma-rays through photon background is

$$\lambda_{\gamma\gamma} = \frac{1}{\sigma_{\gamma\gamma} n_{ph}} \approx 10^4 \left[\frac{n_{ph}}{10^{21} \text{ cm}^{-3}} \right]^{-1} \text{ cm}$$

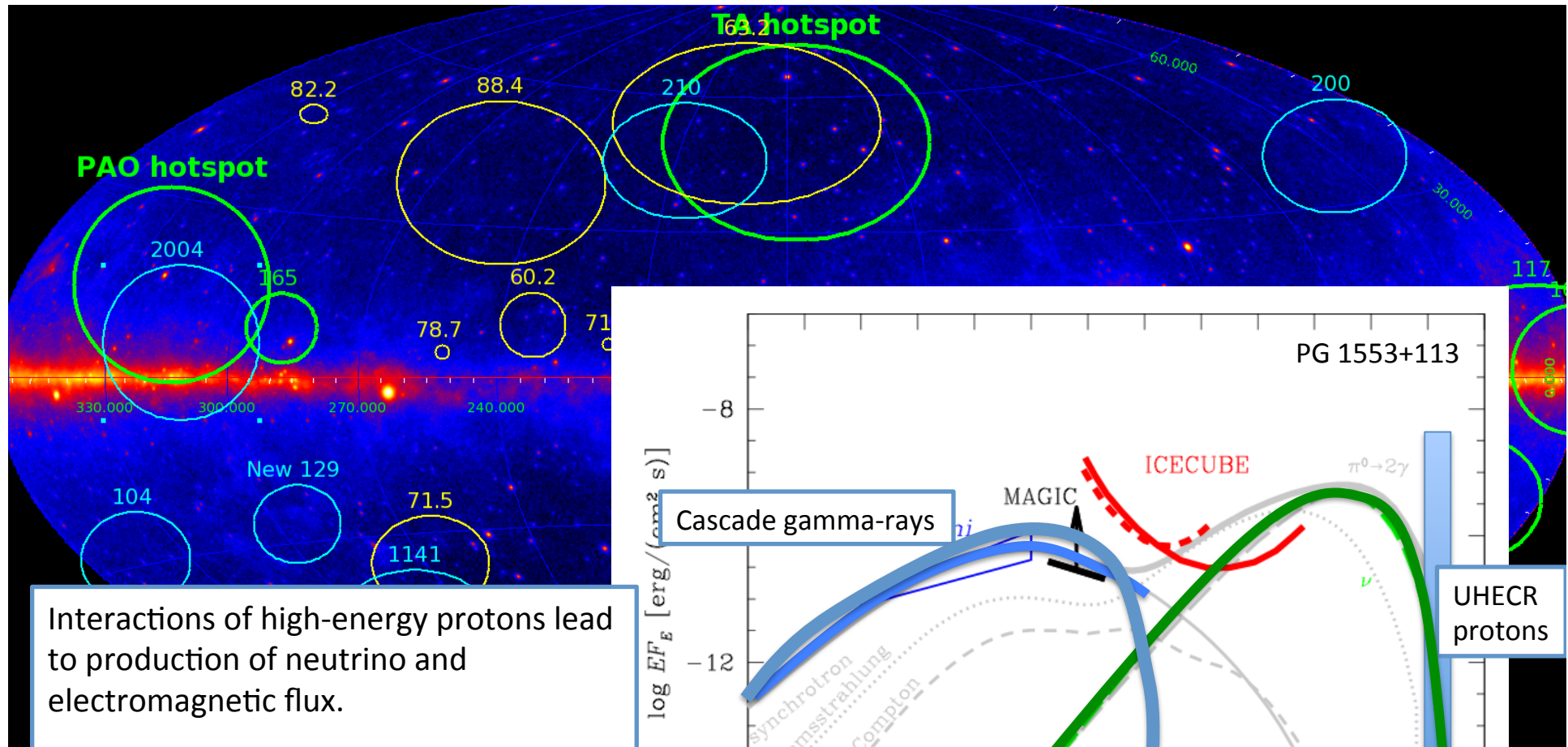
Gamma-rays with multi-GeV energies could hardly escape from the vicinity of the black hole surrounded by a luminous accretion disk.

Gamma-rays produced in pp interactions initiate electromagnetic cascade which transfers power to the energy band below the pair production threshold.

Number density of low-energy photons close to the black hole is

$$n_{UV} = \frac{L}{4\pi R^2 E_{\gamma 2}} \\ \approx 10^{18} \left[\frac{L}{10^{45} \text{ erg/s}} \right]^2 \left[\frac{R}{10^{13} \text{ cm}} \right]^{-2} \text{ cm}^{-3}$$

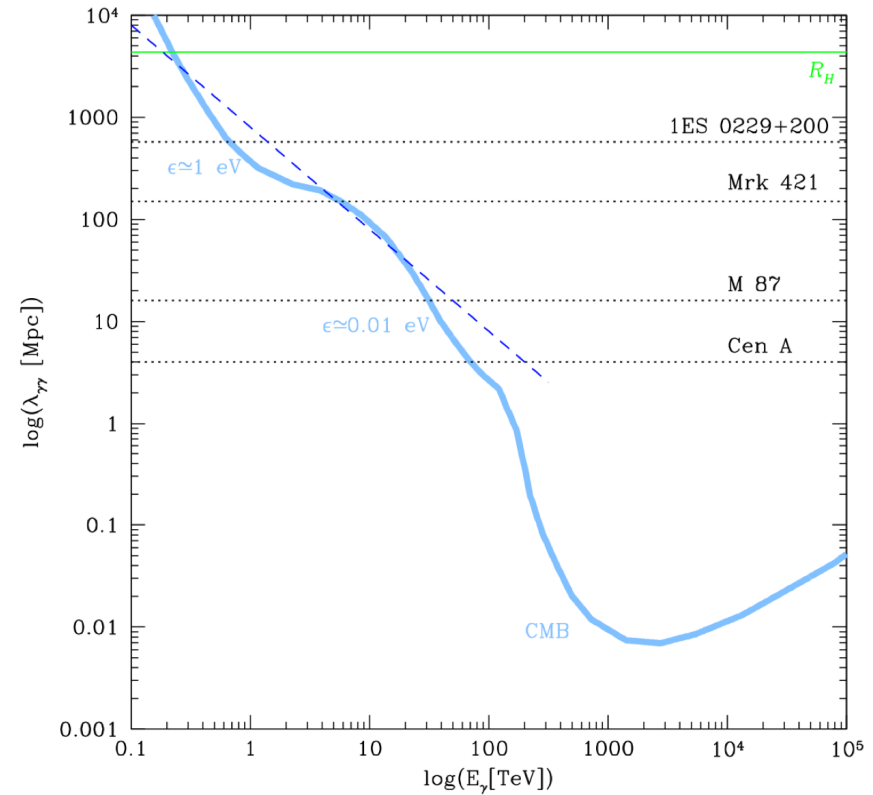
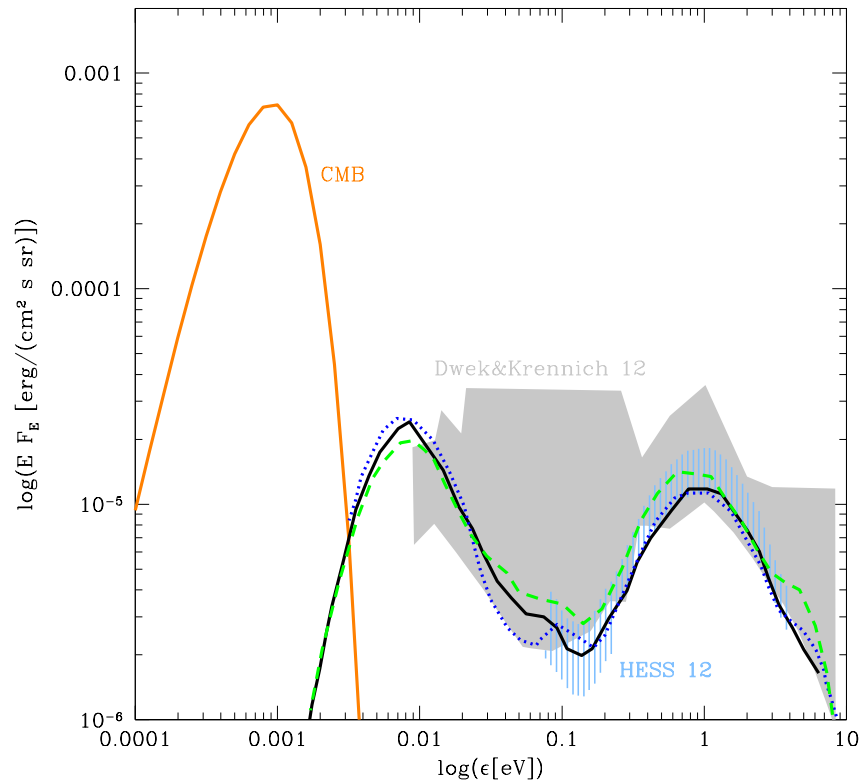
AGN as potential sources of neutrinos



Interactions of high-energy protons lead to production of neutrino and electromagnetic flux.

The overall power of neutrino and electromagnetic flux is comparable, but they are emitted in different energy bands.

Electromagnetic cascade in the intergalactic medium



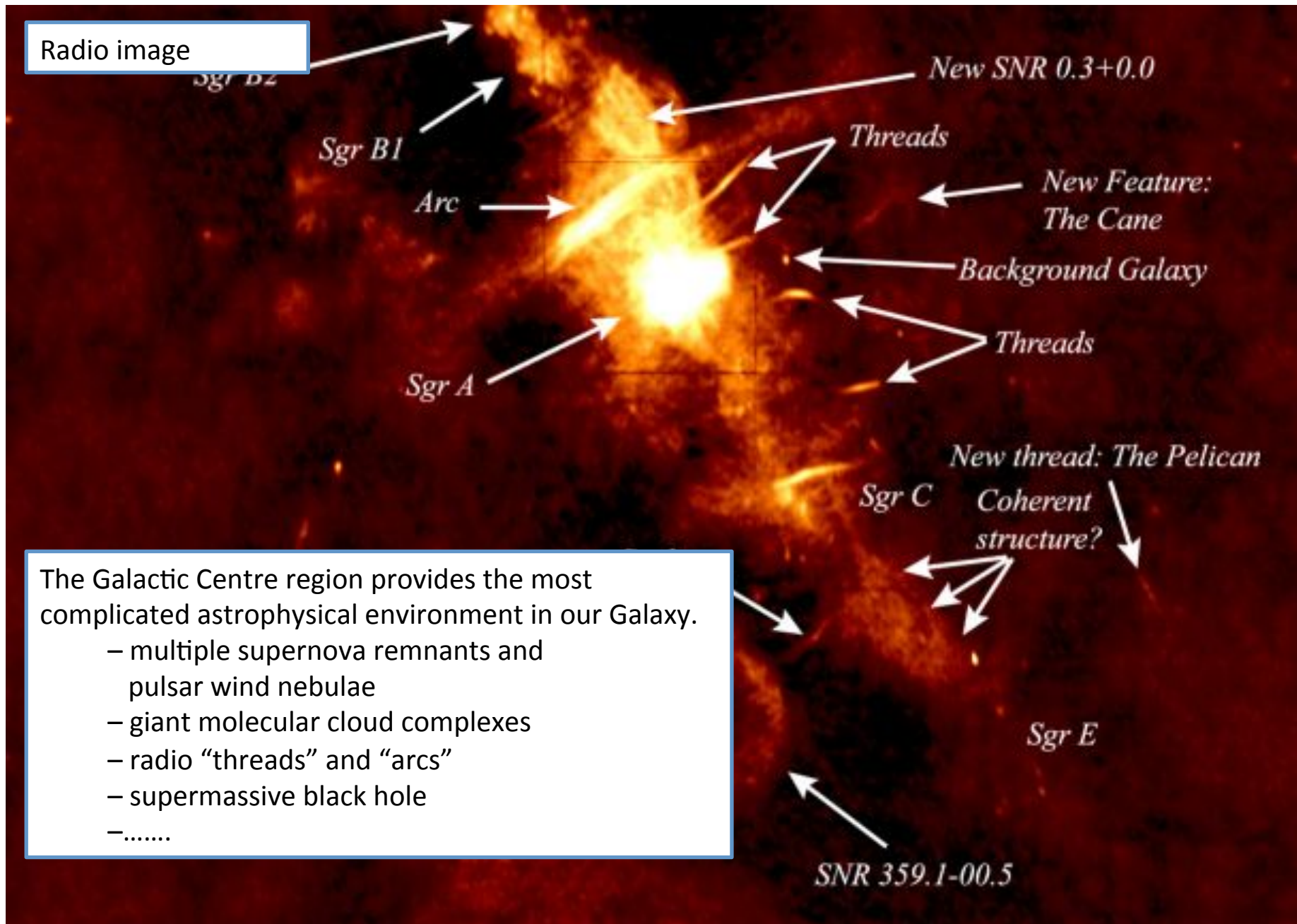
Highest energy gamma-rays are also absorbed on the way from the source to the Earth in interactions with Extragalactic Background Light photons (infrared – visible band)

$$E_{\gamma 1} \geq \frac{m_e^2}{E_{\gamma 2}} \sim 0.25 \left[\frac{E_{\gamma 2}}{1 \text{ eV}} \right]^{-1} \text{ TeV}$$

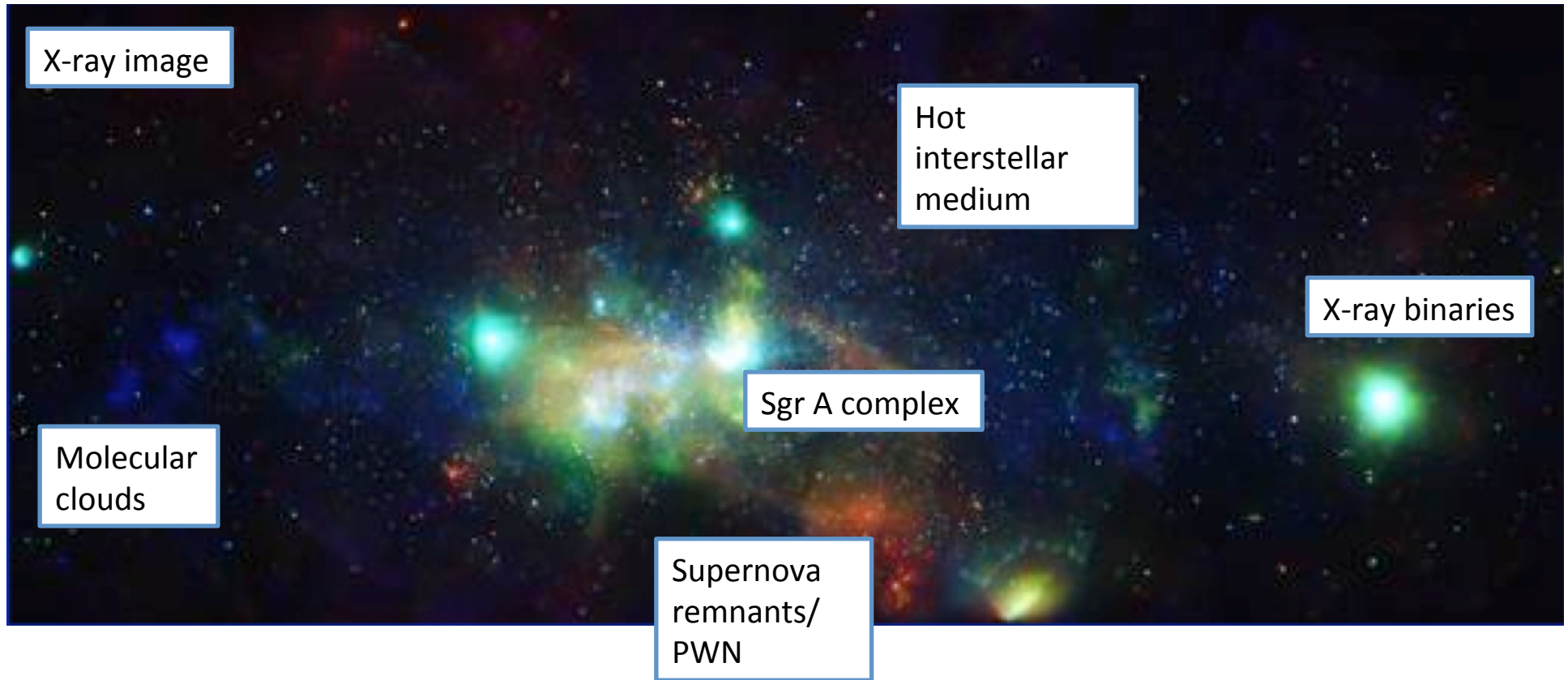
Photon mean free path is $\lambda_{\gamma\gamma} \approx 300(n_{ph} / 10^{-2} \text{ cm}^{-3})^{-1} \text{ Mpc}$ which is shorter than the distance to blazars. Gamma-gamma pair production leads to suppression of gamma-ray flux from distant sources.

The Galactic Centre

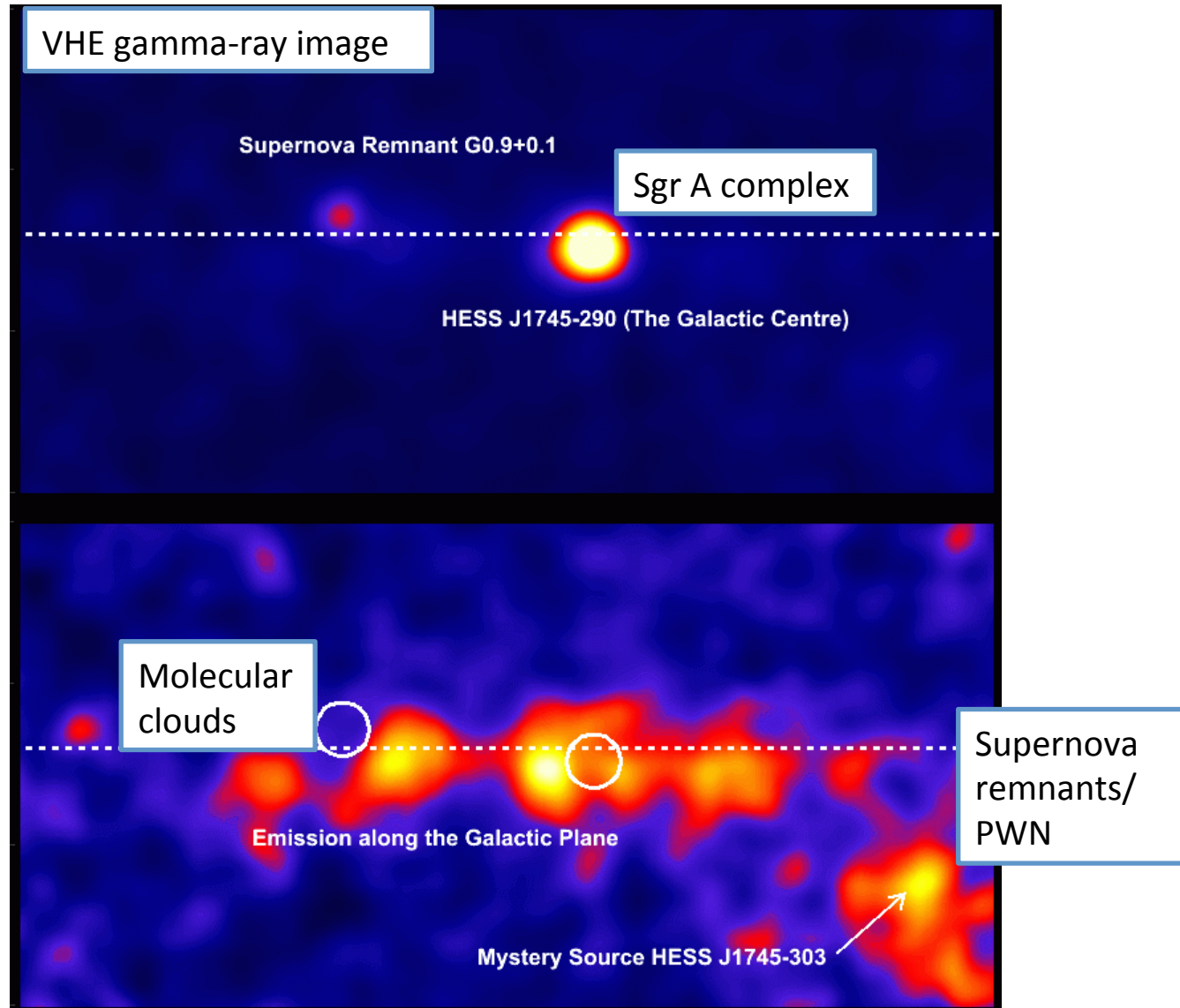
The Galactic Centre



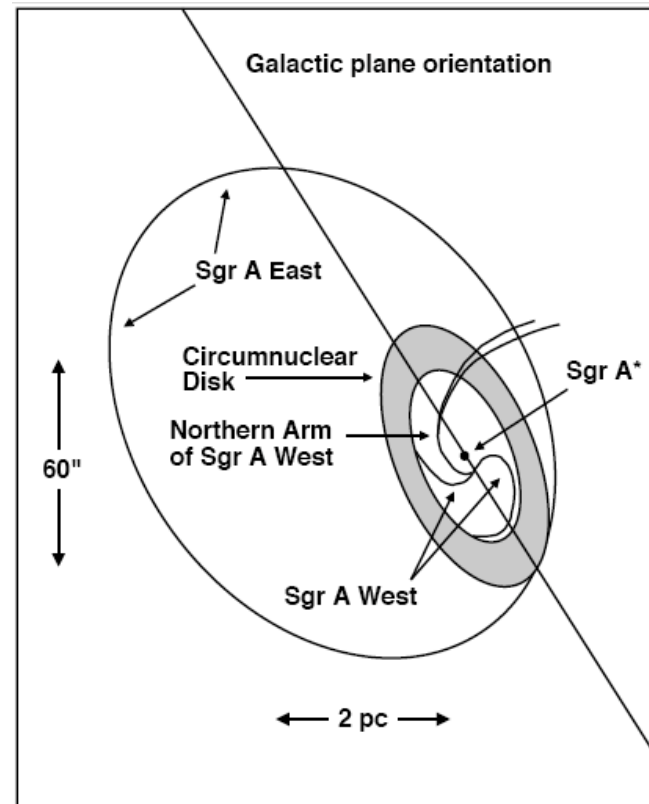
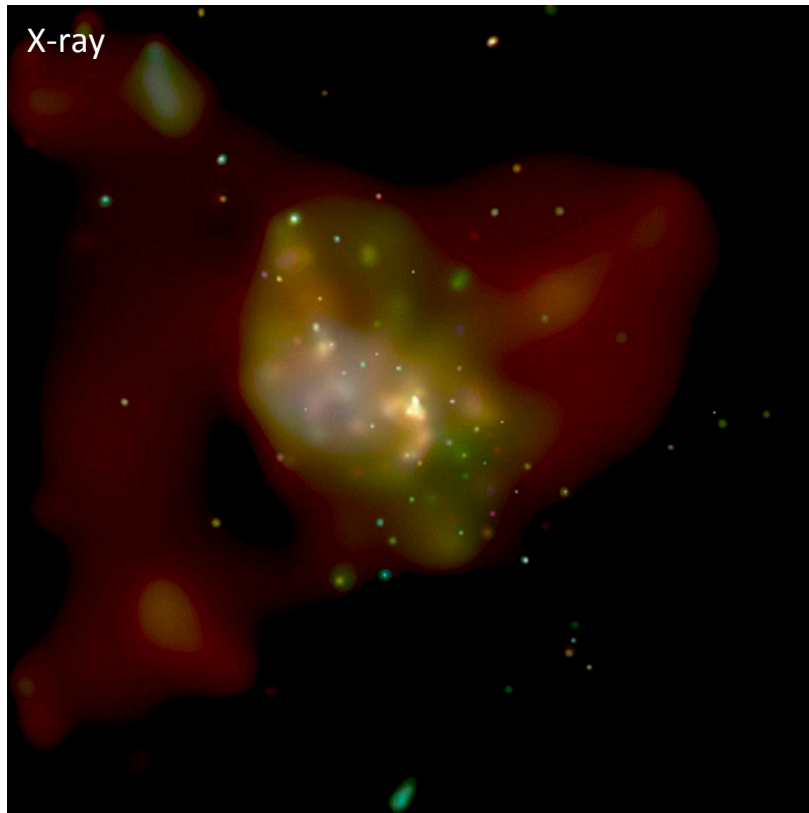
The Galactic Centre



The Galactic Centre

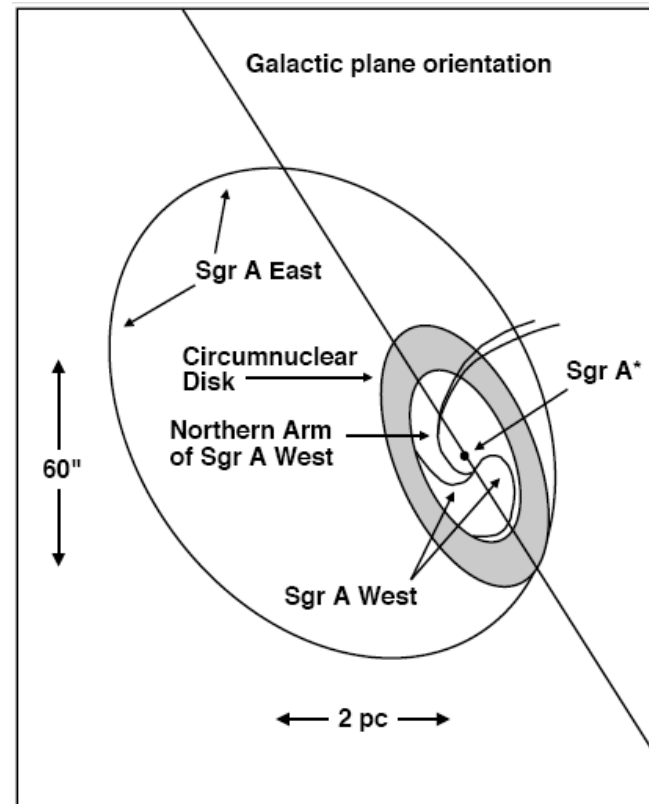
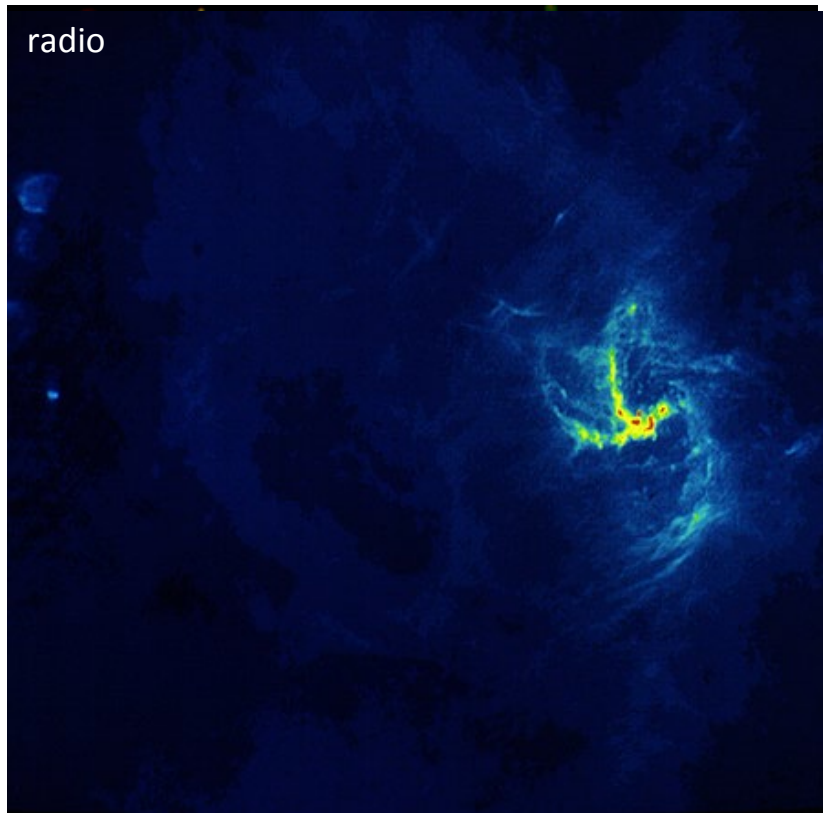


Sgr A complex



The Galactic Centre is embedded into extended “bubble like” structure Sgr A East, of the size ~ 10 pc.

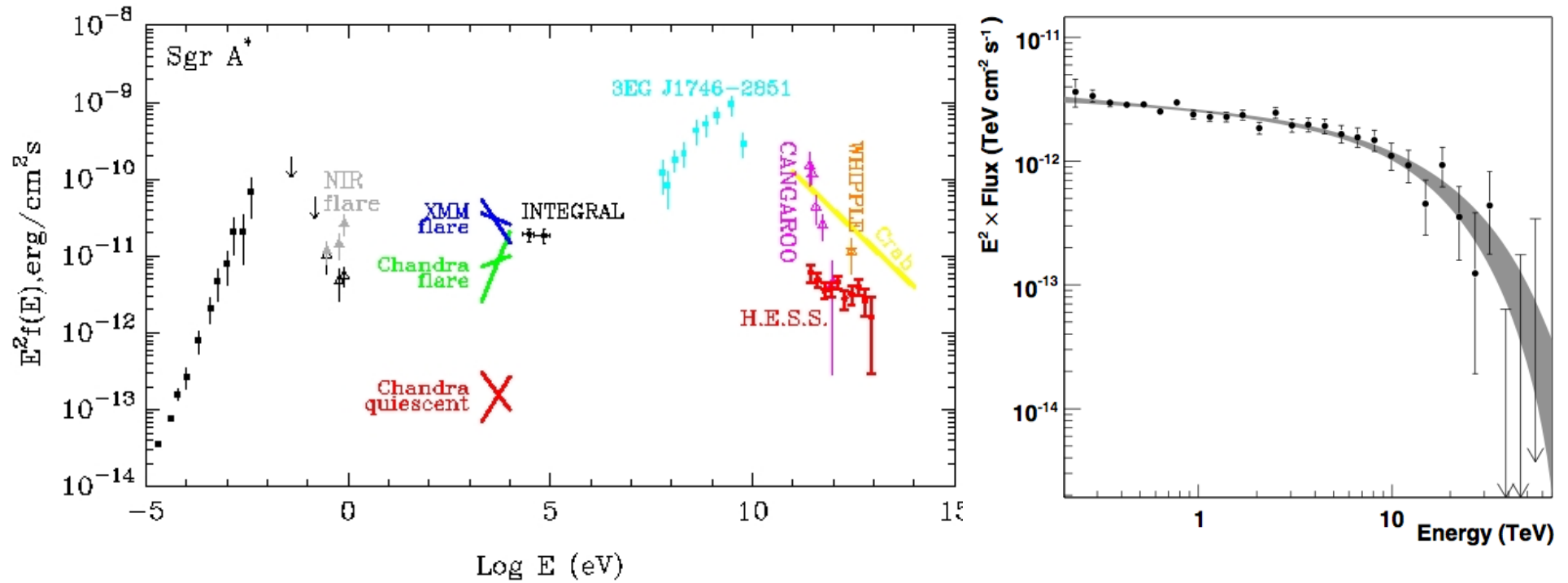
Sgr A complex



The Galactic Centre is embedded into extended “bubble like” structure Sgr A East, of the size ~ 10 pc.

Directly adjacent to the GC is a spiral structure Sgr A West.

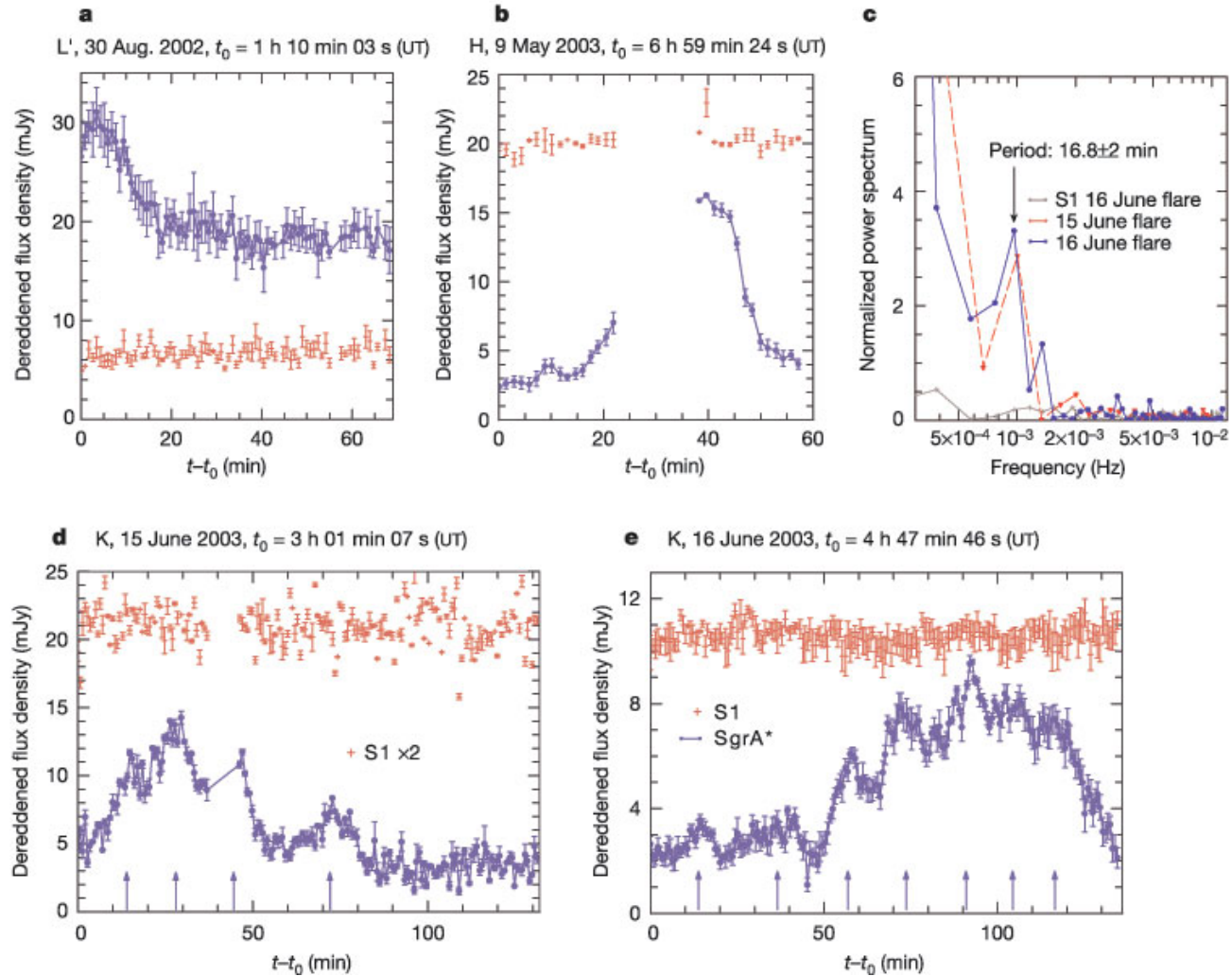
Sgr A*



The Galactic Centre source Sgr A* is a weak non-thermal source with the spectrum extending up to the energy $E \sim 30$ TeV.

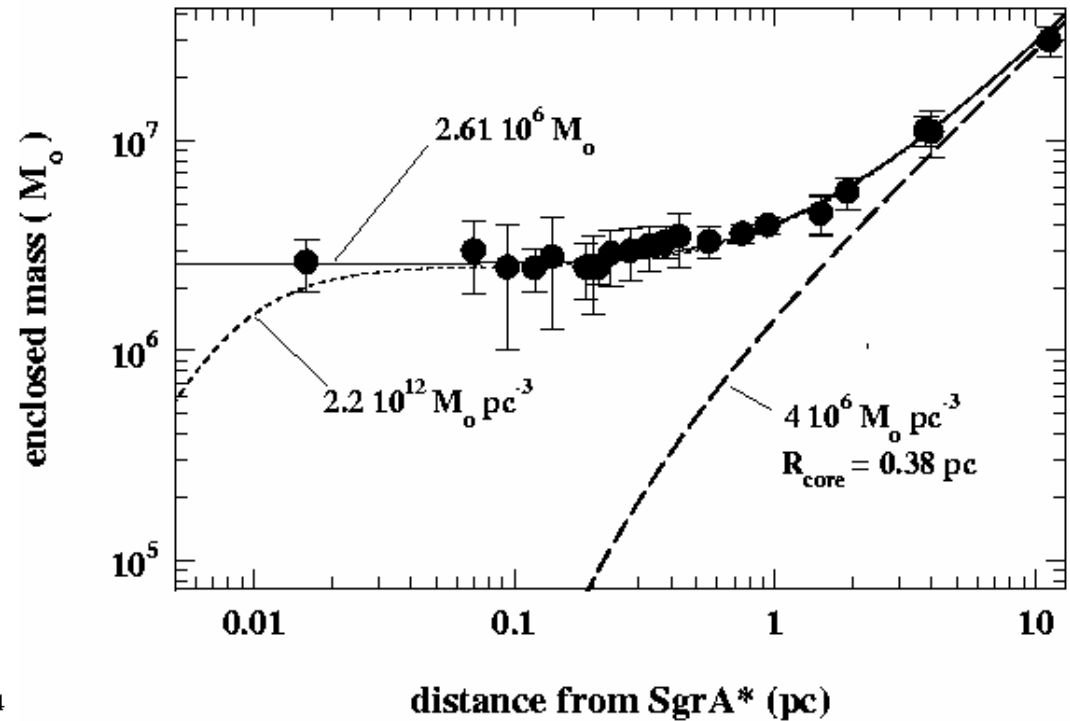
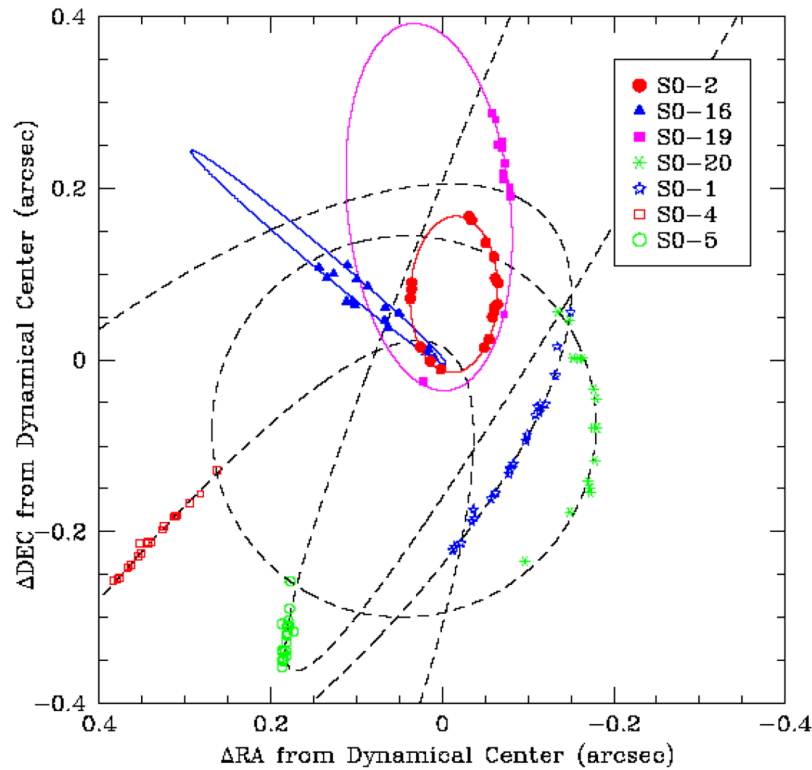
The source luminosity is about $L \sim 10^{36}$ erg/s.

Sgr A*



The source is strongly variable in near-IR and X-ray bands (but not in gamma-rays) on very short time scales, $T \sim 10 \text{ min}$. This limits the source size to be $R < 10^{13} \text{ cm}$

Sgr A*



Study of stellar orbits around the source indicates that it hosts a supermassive black hole of the mass $M \approx 3 \times 10^6 M_{\odot}$

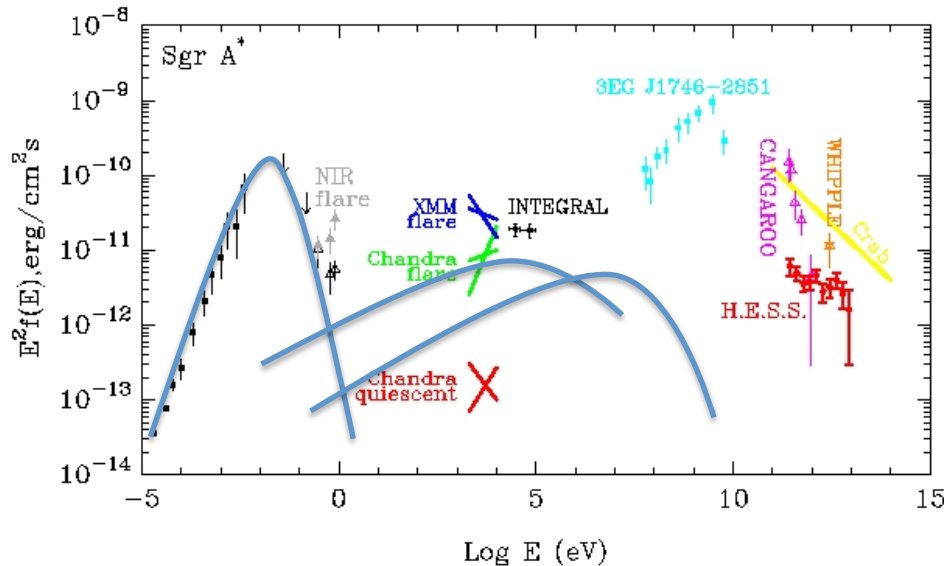
Schwarzschild radius of the black hole is $\sim 10^{12}$ cm. X-ray and infrared variability time scale indicates that emission is produced in the direct vicinity of the black hole.

Eddington luminosity of the black hole is

$$M \approx 10^{44.5} \left[\frac{M}{3 \times 10^6 M_{\odot}} \right] \text{ erg/s}$$

The observed luminosity is 8 orders of magnitude below. This indicates that either the accretion rate on the black hole is very low or that the accretion flow is “**radiatively inefficient**”.

Radiatively inefficient accretion in Sgr A*



If the accretion rate is low, the density of accretion flow is low and particles are not cooled efficiently down from their virial temperature

$$T \sim \frac{GMm}{R} \approx m \left(\frac{R}{R_{BH}} \right)^{-1}$$

Close to horizon, the temperature of protons reaches $\sim 0.1-1$ GeV and temperature of electrons is $\sim 1-100$ MeV (exchange of energy with protons would heat the electrons to higher temperatures).

The accretion rate could be estimated known the density $n \sim 10^2 \text{ cm}^{-3}$ and temperature $T \sim 0.1-1 \text{ keV}$ of the interstellar medium.

The accretion radius is determined by the condition $T \sim G_N Mm / R_{acc}$. Matter is removed from inside the accretion radius with the free fall velocity $v_{acc} \sim \sqrt{GM / R_{acc}}$. Numerical estimate gives

$$\dot{M} \sim 10^{-4} M_{\odot} / \text{yr}$$

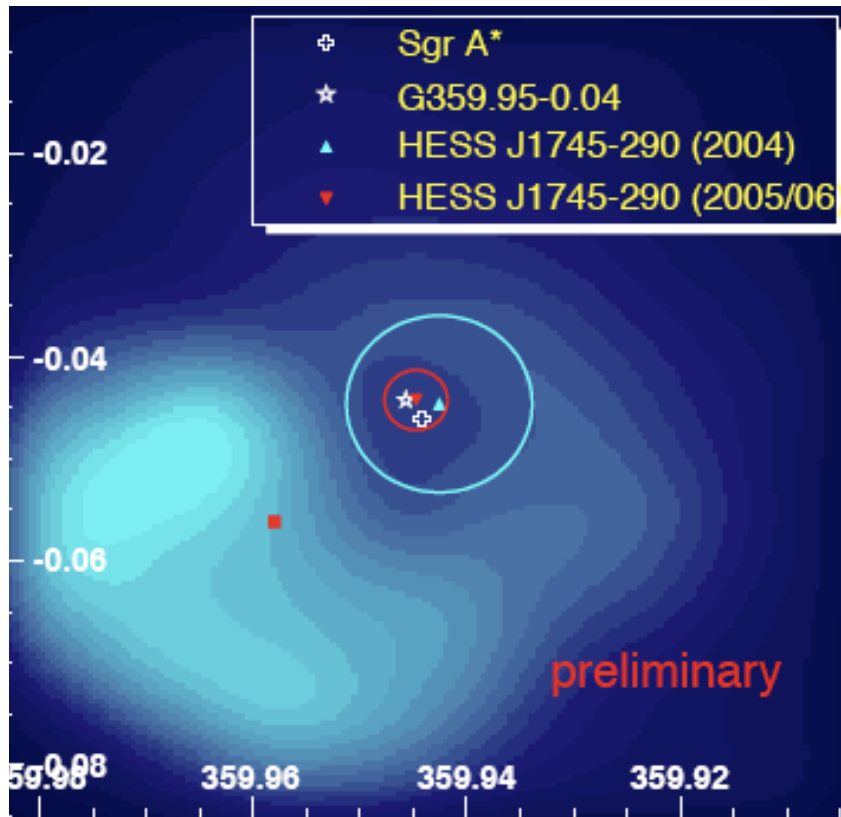
If the accretion would be radiatively efficient, the luminosity of the source would be

$$L \sim 0.1 \dot{M} \sim 10^{41} \text{ erg/s}$$

Mildly relativistic electrons emit synchrotron – inverse Compton and Bremsstrahlung emission.

Comparison of synchrotron and inverse Compton luminosity provides an estimate of magnetic field $B \sim 10 \text{ G}$. Infrared emission component could be identified with the synchrotron emission from GeV electrons. X-ray with the inverse Compton emission by the same electrons.

Particle acceleration in the Galactic Centre



A naïve estimate of the maximal attainable energies of particles is

$$E_{max} \approx 3 \times 10^{15} \left[\frac{B}{10 \text{ G}} \right] \left[\frac{R}{10^{12} \text{ cm}} \right] \text{ eV}$$

However, it is not clear if the non-variable gamma-ray component originates from the accretion flow, i.e. if there is particle acceleration mechanism operating near the black hole.

The non-variable gamma-ray source could well be extended, because high-energy electrons and protons could, most probably escape from the Low-density accretion flow ($n \sim 10^8 \text{ cm}^{-3}$ close to the horizon). Pion production cooling time for protons is $t_{pp} = (k\sigma_{pp}n)^{-1} \sim 1 \text{ yr}$ which is much larger than the escape time from the innermost part of the accretion flow.

Sgr A* possibly provides a constant source of high-energy particles diffusing into the interstellar medium.

Summary

